International Journal of Modern Physics E

Universality of nucleon-nucleon short-range correlations and nucleon momentum distributions

Massimiliano Alvioli

CNR-IRPI, Istituto di Ricerca per la Protezione Idrogeologica, Via Madonna Alta 126, I-06128, Perugia, Italy

Claudio Ciofi degli Atti*

Istituto Nazionale di Fisica Nucleare, Sezione di Perugia, c/o Department of Physics, University of Perugia, Via A. Pascoli, I-06123, Perugia, Italy

Leonid P. Kaptari

Bogoliubov Lab. Theor. Phys., JINR, 141980, Dubna, Russia

Chiara Benedetta Mezzetti

Department of Chemistry and Industrial Chemistry, University of Pisa, Via Risorgimento 35, I-56126, Italy, and
Consorzio Interuniversitario Nazionale per la Scienza e Tecnologia dei Materiali, via G. Giusti 9, Pisa, I-50121, Italy, and Istituto Nazionale di Fisica Nucleare, Sezione di Perugia, Via A. Pascoli, I-06123, Perugia, Italy

Hiko Morita

Sapporo Gakuin University, Bunkyo-dai 11, Ebetsu 069-8555, Hokkaido, Japan

By analyzing recent microscopic many-body calculations of few-nucleon systems and complex nuclei performed by different groups in terms of realistic nucleon-nucleon (NN) interactions, it is shown that NN short-range correlations (SRCs) have a universal character, in that the correlation hole that they produce in nuclei appears to be almost A-independent and similar to the correlation hole in the deuteron. The correlation hole creates high-momentum components, missing in a mean-field (MF) description and exhibiting several scaling properties and a peculiar spin-isospin structure. In particular, the momentum distribution of a pair of nucleons in spin-isospin state $(ST) = (10)$, depending upon the pair relative (k_{rel}) and center-of-mass (c.m.) ($K_{c.m.}$) momenta, as well as upon the angle Θ between them, exhibits a remarkable property: in the region $k_{rel} \gtrsim 2\, fm^{-1}$ and $K_{c.m.} \lesssim 1\, fm^{-1}$, the relative and c.m. motions are decoupled and the two-nucleon momentum distribution factorizes into the deuteron momentum distribution and an A-dependent momentum distribution describing the c.m. motion of the pair in the medium. The impact of these and other properties of one- and two- nucleon momentum distributions on various nuclear phenomena, on ab initio calculations in terms of low-momentum interactions, as well as on ongoing experimental investigations of SRCs, are briefly commented.

*Contact person: ciofi@pg.infn.it

Keywords: Many-body approaches; NN interactions; Short Range Correlations; Momentum Distributions

1. Introduction

It is well known that many low-energy properties of nuclei can be successfully explained in terms of the independent motion of nucleons in a MF created by their mutual interaction (see, e.g.[1]). Recently, however, it became possible to investigate nuclear structure at high values of energy and momentum transfers, probing inter-nucleon distances of the order of the nucleon radius ($\simeq 1fm$) (see e.g.[2] and references therein quoted). This would make it possible to answer longstanding questions concerning the structure of nuclei at short distances, e.g.:

(1) *what are the quantitative limits of validity of the MF picture of nuclei?*
(2) *Does the strong short-range repulsion characterizing modern NN interactions*[3–7] *manifest itself in strong NN SRCs in the nuclear medium, i.e. strong deviations from the independent particle motion (IPM) at short inter-nucleon distances? Are SRCs limited to two-nucleon correlations, reminiscent of the ones occurring in the deuteron, or many-nucleon SRCs should also be considered?*
(3) *Do nucleon and meson remain the dominant effective degrees of freedom (d.o.f.) in the short-region domain of nuclei, or quark and gluon d.o.f. have to be taken explicitly into account?*
(4) *Do the details of the short-range structure of nuclei affect unconventional nuclear processes like, e.g., the structure of cold hadronic matter at high densities or high-energy processes like nucleon-nucleus and nucleus-nucleus scattering at relativistic energies?*

Unveiling the details of the short-range structure of nuclei is a fundamental task of nuclear physics. As a matter of fact, it should be kept in mind that the strong repulsive core in the NN potential, resulting from the analysis of NN elastic scattering data, is introduced by means of various form factors that leave a certain degree of arbitrariness, leading to different short-range behaviors of various NN interaction models. Moreover, elastic on-shell NN scattering cannot in principle determine the details of the NN interaction in medium, because two nucleons that experience interaction with surrounding partners, are off-the-energy shell. As a result, a family of different phase-equivalent potentials can be derived (see, e.g.[8–10]) that may produce different behaviors of the nuclear wave function at short distances (see e.g.[11]). It should also be stressed that recent *ab initio* many-body approaches (e.g. the Unitary Correlation Operator[12] or the No-Core Shell Model[13] ones) that successfully describe many low-energy properties of nuclei, are based upon various renormalization group (RG) methods (see e.g. Ref.[14–16]) producing phase equivalent soft NN interactions allowing one to readily diagonalize the many-nucleon Hamiltonian that would be extremely difficult to diagonalize by using the original bare interaction. In

these approaches, if high-momentum properties have to be evaluated it is necessary to evolve high-momentum operators within a low-momentum theory, which is no easy task, though important progress is being done recently.[17–19] It is not the aim of this review to discuss these approaches, as well modern many-body theories (for a recent review see Ref.[20]) based upon effective interactions derived from chiral perturbation theory (see e.g.[8,9]), where short-range dynamics is described in terms of contact interactions amongst nucleons. In the present report we focus on the effects produced by the free short-range NN interaction on various nuclear properties and phenomena, i.e. we focus on SRCs, whose theoretical and experimental investigations are ultimately aimed at providing information on the details of in-medium short range NN dynamics.

The importance of studying SRCs was stressed more than fifty years ago (see e.g.[21,22]) but it was only recently that, thanks to the enormous progress made by many-body theories and experimental techniques, the theoretical and experimental studies of SRCs were placed on robust grounds.

This report is mainly addressed at providing a critical overview of recent theoretical calculations demonstrating a universal character of SRCs, in that: (i) in coordinate space they produce in the two-nucleon density at small relative distances a correlation hole (a region not accessible to nucleons), exhibiting, apart from normalization factors, very mild dependence upon the atomic weight A and essentially resembling the correlation hole in the deuteron; (ii) the correlation hole, in turn, generates in the momentum distributions high-momentum components, missing in MF momentum distributions, and also exhibiting, to a large extent, independence upon A and several interesting scaling properties. Our report is organized as follows: in Section 2 a review is presented of modern many-body approaches to the calculation of nuclear properties in terms of realistic NN interactions and their prediction about the short-range structure of nuclei; Section 3 shows how the action of SRCs affects the number of NN pairs in a given spin (S) and isospin (T) state (ST); an exhaustive illustration of the properties and spin-isospin structure of the one-body momentum distributions, related to to the spin-isospin structure of SRCs is presented in Section 4; calculations of two-body momentum distributions are reviewed in Section 5, and one- and two-nucleon spectral functions are briefly discussed in Section 6; the Conclusions are presented in Section 7.

2. Ab initio solutions of the nuclear many-body problem and theoretical predictions of SRCs in configuration space

2.1. *The standard model of nuclei*

A description of nuclei in terms of quark and gluon d.o.f. implies the solution of non perturbative QCD problems, a very difficult and yet unsolved task. However, as in the case of various many-body systems composed of particles having their own structure, many-nucleon systems could be viewed as systems of point-like particles interacting via proper effective interactions that incorporate the leading d.o.f. of the

system that, in case of nuclei, are the nucleon and exchanged boson ones. However, the reduction of a field theoretical problem to a non-relativistic potential description generates two-, three-,..., A-body interactions, so that the general potential energy operator assumes the following form

$$\widehat{V}(\mathbf{x}_1, \mathbf{x}_2, \mathbf{x}_3, \ldots, \mathbf{x}_A) = \sum_{n=2}^{A} \hat{v}_n(\mathbf{x}_1, \ldots \mathbf{x}_n), \tag{1}$$

where $\mathbf{x}_i \equiv \{\mathbf{r}_i, \mathbf{s}_i, \mathbf{t}_i, \}$ denotes the nucleon generalized coordinate, including spatial, spin and isospin coordinates. The relative weight of the various components in Eq. (1) has been estimated many years ago in Ref.,[23] arguing that the relative strength between two- and n-body interactions should obey the following qualitative relation

$$(n-body\ potential) \simeq \left(\frac{v_N}{c}\right)^{(n-2)} \times (two-body\ potential), \tag{2}$$

where v_N denotes the average nucleon velocity in a nucleus and c the velocity of light. Taking $v_N \simeq 0.1c$, one is led to the conclusion that the two-nucleon interaction is the dominant one. Though such a statement is qualitatively correct, it is nowadays well established that three-nucleon potentials have to be considered in order to explain the ground-state energy of light nuclei,[24–26] with four-nucleon interactions playing only a minor role[24] (for a recent review on three- and more-nucleon forces see Ref.[27]). Therefore the non-relativistic Schrödinger equation assumes the following form

$$\left[\sum_i \frac{\hat{\mathbf{p}}_i^2}{2\,m_N} + \sum_{i<j} \hat{v}_2(\mathbf{x}_i, \mathbf{x}_j) + \sum_{i<j<k} \hat{v}_3(\mathbf{x}_i, \mathbf{x}_j, \mathbf{x}_k)\right] \Psi_f^A(\{\mathbf{x}\}_A) = E_f^A\, \Psi_f^A(\{\mathbf{x}\}_A), \tag{3}$$

where $\{\mathbf{x}\}_A \equiv \{\mathbf{x}_1, \mathbf{x}_2, \mathbf{x}_3, \ldots, \mathbf{x}_A\}$ denotes the set of A generalized coordinates (the spatial coordinates satisfying the condition $\sum_{i=1}^{A} \boldsymbol{r}_i = 0$) and f denotes the complete set of quantum numbers of state f. Eq. (3) will be referred to as the *Standard Model* of nuclei and in what follows we will be mainly interested in the ground-state wave function $\Psi_{f=0}^A \equiv \Psi_0$. Once the interactions are fixed, Eq. (3) should be solved *ab initio*, i.e. without any significant approximation which could mask or distort the main features of Ψ_n. In what follow we will consider modern 2N bare interactions having the following general form

$$\hat{v}_2(\mathbf{x}_i, \mathbf{x}_j) = \sum_{p=1}^{m} v^{(p)}(r_{ij}) \hat{\mathcal{O}}_{ij}^{(p)} \qquad r_{ij} \equiv |\boldsymbol{r}_i - \boldsymbol{r}_j|, \tag{4}$$

like, e.g., the AV18[5] ($m = 18$) and AV8$'$[6] ($m = 8$) interactions, whose main components are:

$$\begin{aligned} &\mathcal{O}_{ij}^{(1)} = 1,\ \mathcal{O}_{ij}^{(2)} = \boldsymbol{\sigma}_i \cdot \boldsymbol{\sigma}_j,\ \mathcal{O}_{ij}^{(3)} = \boldsymbol{\tau}_i \cdot \boldsymbol{\tau}_j,\ \mathcal{O}_{ij}^{(4)} = (\boldsymbol{\sigma}_i \cdot \boldsymbol{\sigma}_j)(\boldsymbol{\tau}_i \cdot \boldsymbol{\tau}_j) \\ &\mathcal{O}_{ij}^{(5)} = \hat{S}_{ij},\ \mathcal{O}_{ij}^{(6)} = \hat{S}_{ij} \boldsymbol{\tau}_i \cdot \boldsymbol{\tau}_j, \end{aligned} \tag{5}$$

with

$$\hat{S}_{ij} = 3(\hat{\boldsymbol{r}}_{ij} \cdot \boldsymbol{\sigma}_i)(\hat{\boldsymbol{r}}_{ij} \cdot \boldsymbol{\sigma}_j) - \boldsymbol{\sigma}_i \cdot \boldsymbol{\sigma}_j. \tag{6}$$

As for 3N potentials, several models have been proposed in order to reproduce the binding energy of few-nucleon systems, that are underbound by about $0.2 - 0.3$ MeV per particle when only 2N interactions are used (see e.g.[28]). Within the MF approximation, $\sum_{i<j} \hat{v}_2(\mathbf{x}_i, \mathbf{x}_j) + \sum_{i<j<k} \hat{v}_3(\mathbf{x}_i, \mathbf{x}_j, \mathbf{x}_k) \Rightarrow \sum_i U(\mathbf{x}_i)$, the ground-state solution of Eq. (3) is an antisymmetrized product of single particle wave functions ϕ_{α_i}, i.e.

$$\Psi_0(\{\mathbf{x}\}_A) \Rightarrow \Phi_0(\{\mathbf{x}\}_A) = \hat{\mathcal{A}} \prod_i^A \phi_{\alpha_i}(\mathbf{x}_i) = \Phi_{0p0h}(\{\mathbf{x}\}_A), \tag{7}$$

where $\Phi_{0p0h}(\{\mathbf{x}\}_A)$ is a Slater determinant with zero particle, zero hole (0p-0h) excitations, i.e. with all states below the Fermi (F) level occupied and those above it empty ($\phi_{\alpha_i} = 0$ if $\alpha_i > \alpha_F$). The general solution of Eq. (3) includes, on the opposite, a huge number of Slater determinants describing *np-nh* excitations generated by SRCs

$$\Psi_0(\{\mathbf{x}\}_A) = c_0\, \phi_{0p0h}(\{\mathbf{x}\}_A) + c_1\, \Phi_{1p1h}(\{\mathbf{x}\}_A) + c_2\, \Phi_{2p2h}(\{\mathbf{x}\}_A) + \ldots. \tag{8}$$

Ab initio direct solutions of Eq. (3) in terms of bare realistic interactions are possible in the case of few-nucleon systems (A=3, 4) within several approaches (see e.g. Refs.[29–37]). For complex nuclei the fully *ab initio* solutions are still difficult to obtain, but for $A \leq 12$ ground-state energies and excitation spectra were obtained with the AV18 NN interaction plus 3N potentials, by means of the Green Function Monte Carlo (GFMC) method (see e.g. Ref.[38]); for ^{16}O the Variational Monte Carlo (VMC) method has been used,[39] and for $A \geq 16$ the *cluster expansion* approach has been adopted with success.[40,41] The picture that emerges from these calculations is a structure of the ground-state wave function in the following form

$$\Psi_0(\{\mathbf{x}\}_A) \;=\; \hat{F}(\{\mathbf{x}\}_A)\, \Phi_0(\{\mathbf{x}\}_A), \tag{9}$$

where

$$\hat{F}(\{\mathbf{x}\}_A) = \hat{\mathcal{S}} \prod_{i<j} \hat{f}_{ij}(\mathbf{x}_i, \mathbf{x}_j) = \hat{\mathcal{S}} \prod_{i<j} \left[\sum_{n=1}^{m} f^{(n)}(r_{ij}) \hat{\mathcal{O}}_{ij}^{(n)} \right] \tag{10}$$

is a correlation operator introducing SRCs into the MF wave functions Φ_0, $\hat{\mathcal{S}}$ is a symmetrization operator, and $\hat{\mathcal{O}}_{ij}^{(n)}$ is the same operator appearing in Eq. (4). It can be seen that the many-body wave function exhibits a rich correlation structure, the dominant SRC effects arising from the short-range repulsion and the intermediate tensor attraction.

2.2. *The one- and two-body densities and SRCs*

Once the many-body wave function Ψ_0 is at disposal, the relevant quantities of interest are the n-body density, in particular:
1. the one-body non-diagonal spin-isospin independent density:

$$\rho(\boldsymbol{r}_1,\boldsymbol{r}'_1) = A\int \Psi_0^*(\boldsymbol{r}_1,\{\boldsymbol{r}\}_{A-1})\Psi_0(\boldsymbol{r}'_1,\{\boldsymbol{r}\}_{A-1})\prod_{i=2}^{A} d\boldsymbol{r}_i; \tag{11}$$

2. the two-body non-diagonal spin-isospin independent density

$$\rho(\boldsymbol{r}_1,\boldsymbol{r}'_1;\boldsymbol{r}_2,\boldsymbol{r}'_2) = \frac{A(A-1)}{2}\int \Psi_0^*(\boldsymbol{r}_1,\boldsymbol{r}_2,\{\boldsymbol{r}\}_{A-2})\Psi_0(\boldsymbol{r}'_1,\boldsymbol{r}'_2,\{\boldsymbol{r}\}_{A-2})\prod_{i=3}^{A} d\boldsymbol{r}_i; \tag{12}$$

3. the non-diagonal spin-isospin dependent two-body density

$$\rho^{N_1N_2}_{(ST)}(\mathbf{r}_1,\mathbf{r}'_1;\mathbf{r}_2,\mathbf{r}'_2) = \int \psi_0^{A*}(\{\widetilde{\mathbf{x}}\}_A)\sum_{i<j}\hat{P}^S_{ij}\,\hat{P}^T_{ij}\,\widehat{\rho}_{ij}(\mathbf{r}_1,\mathbf{r}'_1;\mathbf{r}_2,\mathbf{r}'_2)\psi_0^A(\{\widetilde{\mathbf{x}}'\}_A)d\boldsymbol{X}; \tag{13}$$

where $d\,\boldsymbol{X}\equiv\prod_{i=1}^{A} d\widetilde{\mathbf{x}}_i d\widetilde{\mathbf{x}}'_i$ and the non-diagonal two-body density operator is

$$\widehat{\rho}_{ij}(\mathbf{r}_1,\mathbf{r}'_1;\mathbf{r}_2,\mathbf{r}'_2) = \delta(\widetilde{\mathbf{r}}_i-\mathbf{r}_1)\delta(\widetilde{\mathbf{r}}_j-\mathbf{r}_2)\delta(\widetilde{\mathbf{r}}'_i-\mathbf{r}'_1)\delta(\widetilde{\mathbf{r}}'_j-\mathbf{r}'_2)\prod_{k\neq\{i,j\}}^{A}\delta(\widetilde{\mathbf{r}}_k-\widetilde{\mathbf{r}}'_k). \tag{14}$$

Here N_1 and N_2 denote the two nucleons in state (ST) and $\hat{P}^{S(T)}_{ij}$ is a projection operator in the state with spin (isospin) S(T). The one-body diagonal $\rho(\boldsymbol{r}_1)$, two-body diagonal $\rho(\boldsymbol{r}_1,\boldsymbol{r}_2)$, half-diagonal $\rho(\boldsymbol{r}_1,\boldsymbol{r}_2;\boldsymbol{r}'_1)$ and $\rho^{N_1N_2}_{(ST)}(\mathbf{r}_1,\mathbf{r}_2;\mathbf{r}'_1)$ densities can easily be obtained from Eqs. (12), (13) and (14), by inserting proper δ-functions into the integrals and properly generalizing the operator (14) (see Ref.[42]).

Let us consider the diagonal two-body density

$$\rho(\boldsymbol{r}_1,\boldsymbol{r}_2) = \sum_{ST}\rho^{N_1N_2}_{(ST)}(\mathbf{r}_1,\mathbf{r}_2) = \rho(\mathbf{r}_{rel},\mathbf{R}_{c.m.}), \tag{15}$$

where the relative (rel) and center-of-mass (c.m.) coordinates are

$$\boldsymbol{r}_{rel} = \boldsymbol{r}_1-\boldsymbol{r}_2\equiv\boldsymbol{r} \qquad \boldsymbol{R}_{c.m.} = \frac{\boldsymbol{r}_1+\boldsymbol{r}_2}{2}\equiv\boldsymbol{R}, \tag{16}$$

and the following relation holds

$$\int\rho(\boldsymbol{r}_1,\boldsymbol{r}_2)d\,\mathbf{r}_1\,d\,\mathbf{r}_2 = \sum_{ST}\int\rho^{N_1N_2}_{(ST)}(\mathbf{r}_1,\mathbf{r}_2)d\,\mathbf{r}_1\,d\,\mathbf{r}_2 = \sum_{ST}N^{N_1N_2}_{(ST)} = \frac{A(A-1)}{2} \tag{17}$$

where $N^{N_1N_2}_{(ST)}$ is the number of NN pairs in state (ST). The relative and *c.m.* two-nucleon densities can then be defined as follows

$$\rho_{rel}(\boldsymbol{r}) = \int\rho(\boldsymbol{r},\boldsymbol{R})\,d\boldsymbol{R} \quad \rho_{c.m.}(\boldsymbol{R}) = \int\rho(\boldsymbol{r},\boldsymbol{R})d\,\boldsymbol{r}. \tag{18}$$

The knowledge of the one- and two-nucleon densities allows one to calculate various nuclear properties, e.g. the ground-state energy and the momentum distributions. The various spin-isospin dependent and independent densities have been calculated by various authors in terms of *ab initio* or, anyway, realistic solutions of Eq. (3) with bare NN realistic interactions. These, which will be discussed in the next Section, provide a very clear definition of SRCs and their effects on NN densities in nuclei.

2.3. *The correlation hole in few-nucleon systems and complex nuclei*

Ab initio calculations with bare realistic interactions show that, apart from an obvious normalization factor counting the different number of pairs in different nuclei,

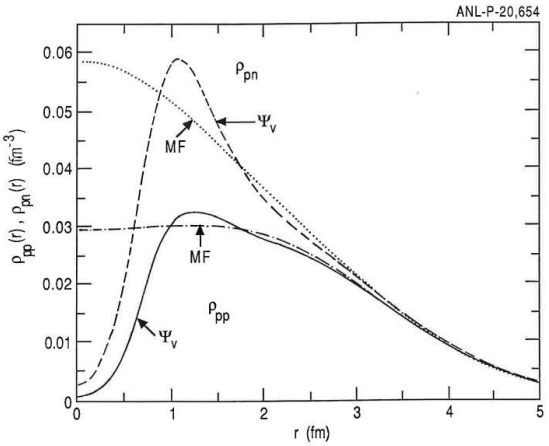

Fig. 1. The two-body density distribution of *pn* and *pp* pairs in ^{16}O corresponding to mean-field (MF) and correlated (Ψ_V) wave functions obtained within the Variational Monte Carlo approach with AV14 NN interaction plus 3N forces (Figure reprinted from.[39] Copyright (1992) by the American Physical Society).

the relative two-body density $\rho_{rel}(r)$ and its spin-isospin components $\rho_{ST}^{N_1N_2}(r)$ exhibits at $r \lesssim 1.5\, fm$ a sharp damping with respect to the analogous MF density. This is exactly the *correlation hole* previously mentioned; it is illustrated in Fig. 1 for the nucleus of ^{16}O. The correlation hole is generated by the cooperation of the short-range repulsion and the intermediate-range tensor attraction of the NN interaction, with the tensor force governing the overshooting at $r \simeq 1.0\, fm$ in the *np* distribution. Figs. 2-4 illustrate the universality of the correlation hole, i.e. its independence upon A. These Figures also demonstrate that different many-body approaches, ranging from the GFMC to proper cluster expansion methods, which may give different results for the ground-state energy, but predict, practically, the same behavior of the correlation hole. In order to be able to obtain information

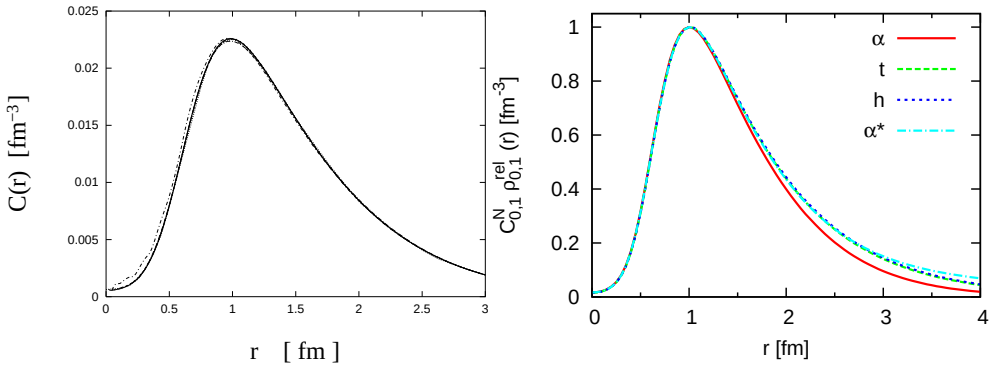

Fig. 2. (**Left**): the relative two-nucleon density in ^{4}He (Eq. (18) with $\rho_{rel}(r) \equiv C(r)$) calculated within six different *ab initio* many-body theories using the AV18 interaction yielding practically undistinguishable results. (Figure reprinted from.[43] Copyright (1992) by the American Physical Society). (**Right**): the relative two-nucleon density (normalized at $r \simeq 1\,fm$) in ^{2}H, ^{3}H, ^{4}He and ^{4}He* for NN pairs in relative S=0 and T=1 state. *Ab initio* calculations within the method of Ref.[35] and AV8′ interaction.[6] (Figure reprinted from.[44] Copyright (2011) by the American Physical Society).

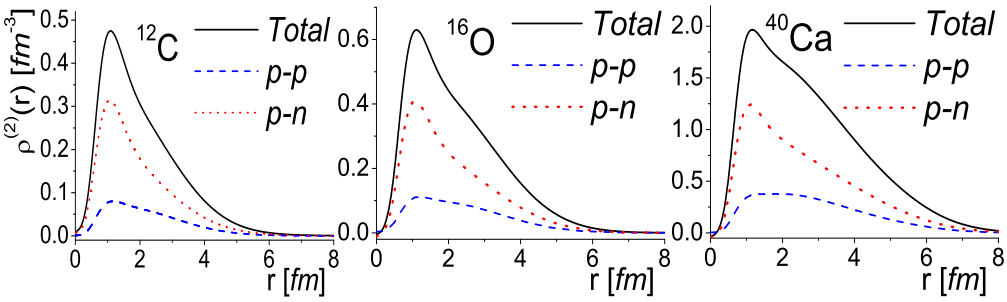

Fig. 3. The two-nucleon density (Eq. (18) with $\rho_{rel}(r) \equiv \rho^{(2)}(r)$) in ^{12}C, ^{16}O, and ^{40}Ca. The separate contributions of *pp* and *nn* densities are also shown. The total density (full line) is given by $\rho^{(2)}(r) = \rho^{(2)}_{pn}(r) + 2\,\rho^{(2)}_{pp}(r)$ because $\rho^{(2)}_{pp}(r) = \rho^{(2)}_{nn}(r)$. Ground-state wave functions from the number-conserving linked-cluster expansion calculation of Ref.,[41] AV8′ interaction.[6] (After Ref.[45]).

about this important feature characterizing the relative NN motion in medium, we have first of all to shift to momentum space, expecting: (i) an increase of nucleon high-momentum components in the ground-state wave function, (ii) peculiar momentum configurations that are missing in a mean-field description, and, eventually, (iii) a variation of the spin-isospin structure of the ground-state wave function. Let us start by discussing the spin-isospin structure of nuclei and how it is affected by SRCs.

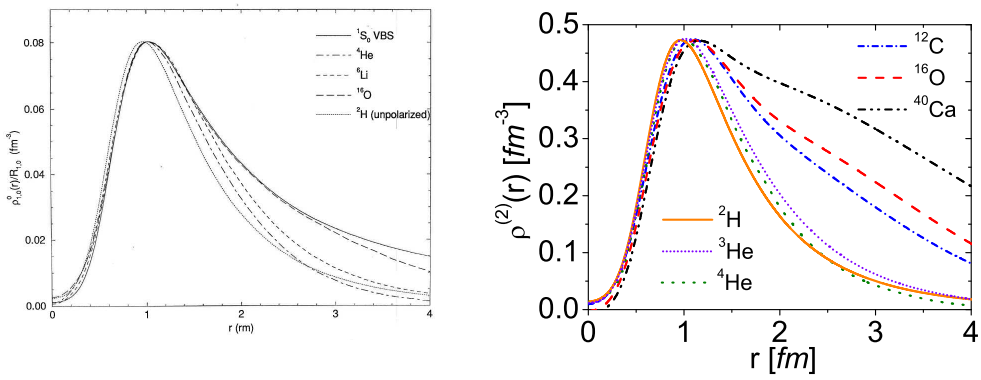

Fig. 4. (**Left**): the relative two-nucleon density (Eq. (18) normalized at $r \simeq 1\,fm$) in ^{2}H, ^{4}He, ^{6}Li and ^{16}O obtained in Ref.[46] within the VMC method and AV18 interaction. (Figure reprinted from.[46] Copyright (1996) by the American Physical Society). (**Right**): the two-nucleon density (Eq. (18) with $\rho_{rel}(r) \equiv \rho^{(2)}(r)$)) obtained with *ab initio* wave functions for ^{3}He and ^4He and within the number-conserving linked-cluster expansion of Ref.[41] and the AV8′ interaction[6] for ^{12}C, ^{16}O and ^{40}Ca .

3. The spin-isospin structure of the nuclear ground state and SRCs

3.1. *The number of spin-isospin pairs in a nucleus*

The quantum numbers that characterize a two-nucleon pair in a nucleus are the relative orbital momentum L, the total spin S and the total isospin T. Pauli principle requires that L + S + T=*odd number*. In a pure shell-model picture and $A \leq 4$ L=0, so that (ST)=(10) and (01), whereas for $A > 4$ we can have both L even, with (ST)=(10) and (01), and L odd, with (ST)=(00) and (11). The deviations from the shell model originating from SRCs, are accompanied, in $A \leq 4$ nuclei, by the creation of (00) and (11) states, and in complex nuclei by a reduction of the number of (01) and (10) states in favor of (11) and (00) states. The number of pairs in different (ST) states in several nuclei given by

$$N_{(ST)} = \int d\boldsymbol{r_1}\, d\boldsymbol{r}_2\, \rho_{(ST)}(\boldsymbol{r}_1;\boldsymbol{r}_2) \tag{19}$$

and calculated by different groups, is reported in Table 1; it can be seen that: (i) SRCs do not practically affect the state (10), but appreciably reduce the state (01), in favor of the (11) state; this is ascribed to a three-body-like mechanism originating from the tensor force[44,46] illustrated in Fig. 5: tensor correlations between particles "2" and "3" generate a spin flip of particle "2", that gives rise to the state (11) between particles "2" and "1" ; (ii) as in the case of the correlation hole, there is again a general agreement between the results by different groups using different many-body approaches, namely: the VMC with various Argonne interactions, in Ref.;[46] the correlated Gaussian basis approach[34] with the V8′ interaction,

Nucleus		(ST) (10)	(01)	(00)	(11)
^{2}H		1	-	-	-
^{3}He	IPM	1.50	1.50	-	-
	SRC[42]	1.488	1.360	0.013	0.139
	SRC[46]	1.50	1.350	0.01	0.14
	SRC[44]	1.489	1.361	0.011	0.139
^{4}He	IPM	3	3	-	-
	SRC[42]	2.99	2.57	0.01	0.43
	SRC[46]	3.02	2.5	0.01	0.47
	SRC[44]	2.992	2.572	0.08	0.428
^{16}O	IPM	30	30	6	54
	SRC[42]	29.8	27.5	6.075	56.7
	SRC[46]	30.05	28.4	6.05	55.5
^{40}Ca	IPM	165	165	45	405
	SRC[42]	165.18	159.39	45.10	410.34

Table 1. The number of pairs $N_{(ST)}$, Eq. (19), in various spin-isospin states in the independent particle model (IPM) and taking into account SRCs within different many-body approaches (see text) with realistic interactions (AV18 and AV8'). (Table reprinted from Ref.[42] Copyright (2013) by the American Physical Society)

in Ref.;[44] the hyperspherical harmonic variational method with the $AV18$ inter-

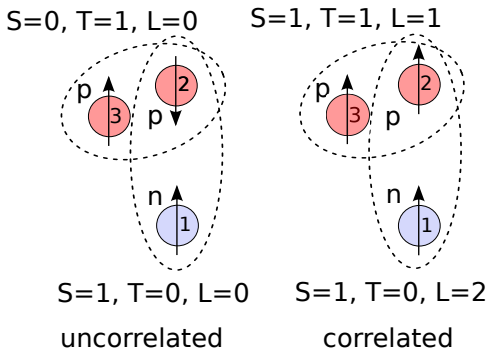

Fig. 5. The three-body mechanism leading to the increase of the number of pairs in $(ST) = (11)$ state (After Ref.[44]). (Figure reprinted from Ref.[44] Copyright (2011) by the American Physical Society).

action in Ref.;[30] the ATMS method of Ref.[31] with the AV8′ interaction and the linked-cluster expansion of Ref.[41] with the AV8′ interaction, in Ref.[42]

4. One-body momentum distributions and SRCs

Let us now discuss how and to what extent SRCs affect the one-body momentum distribution, i. e. the Fourier transform of the non-diagonal one-body density

$$n_A(\boldsymbol{k}_1) = \frac{1}{A(2\,\pi)^3}\int e^{-i\,\boldsymbol{k}_1\cdot(\boldsymbol{r}_1-\boldsymbol{r}'_1)}\rho(\boldsymbol{r}_1,\boldsymbol{r}'_1)d\boldsymbol{r}_1 d\boldsymbol{r}'_1 = \int n_A^{N_1N_2}(\mathbf{k}_1,\mathbf{k}_2)\,d\boldsymbol{k}_2 \quad (20)$$

where $n^{N_1N_2}$ is the two-body momentum distribution to be discussed later on, and $\int n_A(\boldsymbol{k}_1)d\,\boldsymbol{k}_1 = 1$, which is the normalization adopted in the rest of the paper.

4.1. *General definitions and two-nucleon SRC (2N-SRC) configurations*

SRCs considerably increase the high-momentum content of the one-body momentum distributions through the term $\sum_{n=2}^{\infty} c_n\Phi_{npnh}$, in Eq. (8), i.e. via the population of *np-nh* states with momentum much higher than the Fermi momentum $k_F \simeq 1.4fm^{-1}$. SRCs, moreover, generate peculiar wave function configurations

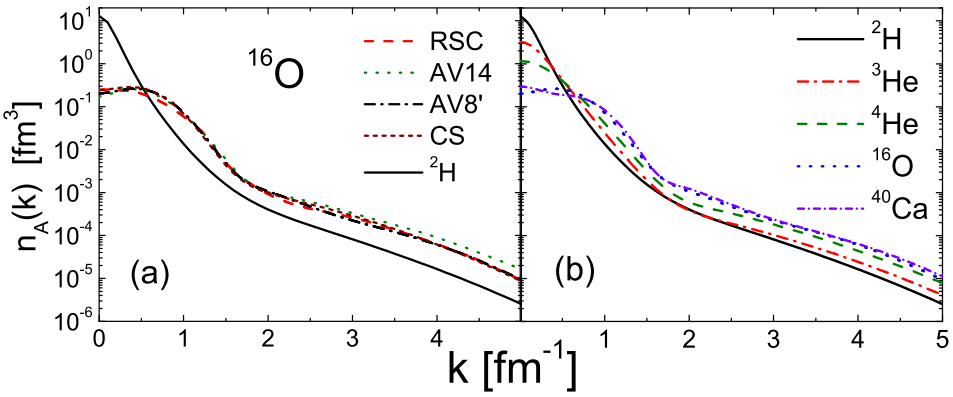

Fig. 6. (**a**): the momentum distribution in ^{16}O calculated with different NN interactions and theoretical approaches: RSC;[48] AV14;[39] AV8'.[41] The phenomenological distribution of Ref.[49] is also shown (CS) and ^{2}H denotes the deuteron momentum distribution. (**b**): the proton momentum distribution of different nuclei calculated within different many-body approaches with equivalent NN interactions, namely the AV18 one, in the case of ^{2}H and ^{3}He, and the AV8′ one, in the case of ^{4}He, ^{16}O, and ^{40}Ca. Hereafter the notation $|\mathbf{k}_1| \equiv k$ will be adopted. (Figure reprinted from.[42] Copyright (2013) by the American Physical Society).

that are missing in a MF description.[47] As a matter of fact, since momentum conservation requires that

$$\sum_{i=1}^{A}\boldsymbol{k}_i = 0 \quad (21)$$

a nucleon with high momentum $\boldsymbol{k}_1$ in a MF configuration is expected to be balanced by the rest of the $(A-1)$ nucleons, i. e.

$$\boldsymbol{k}_1 \simeq -\sum_2^A \boldsymbol{k}_i \qquad \boldsymbol{k}_i \simeq \frac{\boldsymbol{k}_1}{A-1}, \tag{22}$$

whereas in a 2N-SRC configuration one has

$$\boldsymbol{k}_1 \simeq -\boldsymbol{k}_2 \qquad \boldsymbol{K}_{A-2} = \sum_3^A \boldsymbol{k}_i \simeq 0. \tag{23}$$

Therefore 2N-SRCs can be defined as those configurations of a pair of nucleons characterized by *high* relative and *small c.m.* momenta. The quantitative meaning of such a statement will be discussed later on.

4.2. *Recent calculations of the one-body momentum distribution*

A recent systematic analysis of realistic calculations of $n_A(k)$ for A=2, 3, 4, 16, and 40 has been presented in Ref.[42] The results for ^{16}O, performed by different groups, is shown in Fig. 6(**a**), which is aimed at illustrating the convergence of different approaches that use similar NN interactions, whereas Fig. 6(**b**) shows that the high-momentum part of $n_A(\mathbf{k}_1)$ of different nuclei exhibits a qualitative universal scaling behavior. This point will be discussed on a more quantitative level in Section 4.5.

4.3. *The probability of MF and SRC configurations*

The ground-state wave function Ψ_0, solution of Eq. (3) describes both MF and correlated-nucleon motions. The latter, in turn, includes both long- and short-range correlations; long-range correlations (LRC) manifest themselves mostly in open shell nuclei, and are responsible for configuration mixing resulting in partial occupation of states which are empty in a simple independent particle model, with small effects, however, on high-momentum components; SRCs, on the contrary, generate high virtual particle-hole excitations even in closed-shell nuclei, and strongly affect the high-momentum content of the wave function. Therefore, assuming that the momentum distributions could be extracted from some experimental data, we have to figure out a clear cut way to disentangle the momentum content generated by the MF and LRCs from the one arising from SRCs. Denoting by $\{|\psi_f^{A-1}>\}$ the complete set of eigenfunctions of nucleus $(A-1)$ described by the same Hamiltonian of nucleus A, and using the completeness relation

$$\sum_{f=0}^{\infty} |\Psi_f^{A-1}><\Psi_f^{A-1}| = 1, \tag{24}$$

the one-nucleon momentum distribution can be written as follows[50]

$$n_A(\boldsymbol{k}_1) = n_{gr}(\boldsymbol{k}_1) + n_{ex}(\boldsymbol{k}_1), \tag{25}$$

where

$$(2\pi)^3 n_{gr}(\boldsymbol{k}_1) =$$
$$= \sum_{f=0,\sigma_1} \Big| \int e^{i\boldsymbol{k}_1\cdot\boldsymbol{r}_1} d\boldsymbol{r}_1 \int \chi^{\dagger}_{\frac{1}{2}\sigma_1} \Psi^{(A-1)*}_{f=0}(\{\boldsymbol{r}_i\}_{A-1}) \Psi_0(\boldsymbol{r}_1, \{\boldsymbol{r}_i\}_{A-1}) \prod_{i=2}^{A} d\boldsymbol{r}_i \Big|^2 \quad (26)$$

and

$$(2\pi)^3 n_{ex}(\boldsymbol{k}_1) =$$
$$= \sum_{f\neq 0,\sigma_1} \Big| \int e^{i\,\boldsymbol{k}_1\cdot\boldsymbol{r}_1} d\boldsymbol{r}_1 \int \chi^{\dagger}_{\frac{1}{2}\sigma_1} \Psi^{(A-1)*}_{f}(\{\boldsymbol{r}_i\}_{A-1}) \Psi_0(\boldsymbol{r}_1, \{\boldsymbol{r}_i\}_{A-1}) \prod_{i=2}^{A} d\boldsymbol{r}_i \Big|^2 . \quad (27)$$

Here the sum over f stands also for an integral over the continuum final states that are present in Eq. (24). We see that the momentum distribution can be expressed through the overlap integrals between the ground-state wave function Ψ_0 of nucleus A and the wave function $\Psi^{(A-1)}_f$ of the state f of nucleus $(A-1)$. The separation of the momentum distributions in n_{gr} and n_{ex} is particularly useful for $A = 3$, 4 nuclei, i.e. when the excited states of $(A-1)$ are in the continuum. For complex nuclei, where many discrete hole excited states are present, it is more convenient to use another representation where the particle-hole structure of the realistic solutions of Eq. (3) is explicitly exhibited by Eq. (8). Within such a representation, one has[51,52]

$$n_A(\boldsymbol{k}_1) = n_0(\boldsymbol{k}_1) + n_1(\boldsymbol{k}_1), \quad (28)$$

where

$$(2\pi)^3\, n_0(\boldsymbol{k}_1) =$$
$$= \sum_{f\leq F,\sigma_1} \Big| \int e^{i\boldsymbol{k}_1\cdot\boldsymbol{r}_1} d\boldsymbol{r}_1 \int \chi^{\dagger}_{\frac{1}{2}\sigma_1} \Psi^{(A-1)*}_{f}(\{\boldsymbol{r}_i\}_{A-1}) \Psi_0(\boldsymbol{r}_1, \{\boldsymbol{r}_i\}_{A-1}) \prod_{i=2}^{A} d\boldsymbol{r}_i \Big|^2 \quad (29)$$

$$(2\pi)^3\, n_1(\boldsymbol{k}_1) =$$
$$= \sum_{f> F,\sigma_1} \Big| \int e^{i\boldsymbol{k}_1\cdot\boldsymbol{r}_1} d\boldsymbol{r}_1 \int \chi^{\dagger}_{\frac{1}{2}\sigma_1} \psi^{(A-1)*}_{f}(\{\boldsymbol{r}_i\}_{A-1}) \psi_0(\boldsymbol{r}_1, \{\boldsymbol{r}_i\}_{A-1}) \prod_{i=2}^{A} d\boldsymbol{r}_i \Big|^2 . \quad (30)$$

The summation over f in Eq. (29) includes all the discrete shell-model levels below the Fermi level in $(A-1)$ ("hole states" of A), and in Eq. (30) it includes all the discrete and continuum states above the Fermi level created by SRCs. In a fully uncorrelated MF approach, one has

$$n_A(\boldsymbol{k}_1) = n_0(\boldsymbol{k}_1) = \sum_{\alpha\leq F} |\phi_\alpha(\boldsymbol{k}_1)|^2 ; \qquad n_1(\boldsymbol{k}_1) = 0. \quad (31)$$

The modulus squared of the overlap integral represents the weight of the ground and excited virtual states of $(A-1)$ in the ground state of A, so that the quantities

$$\mathcal{P}_{gr(0)} = \int_0^\infty n_{gr(0)}(\boldsymbol{k}_1)\, d\,\boldsymbol{k}_1 \quad \mathcal{P}_{ex(1)} = \int_0^\infty n_{ex(1)}(\boldsymbol{k}_1)\, d\,\boldsymbol{k}_1, \quad (32)$$

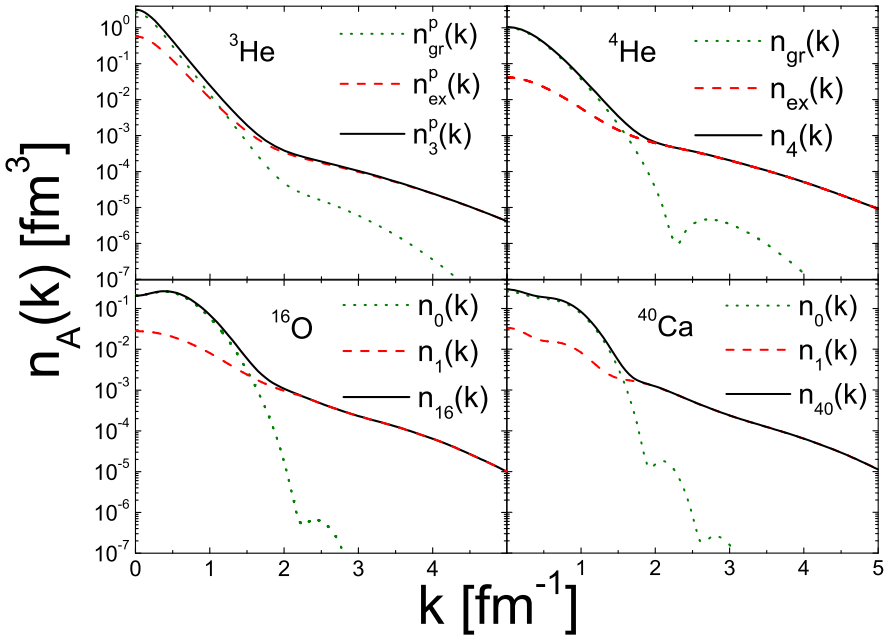

Fig. 7. The proton momentum distribution $n^p_A(k_1) \equiv n_A(k)$ and its separation into the uncorrelated and correlated contributions, Eqs. (25-30), in A=3 (wave function from Ref.,[30] AV18 interaction), A=4 (wave function from Ref.,[31] AV8′ interaction), A= 16 (wave functions from Ref.,[41] AV8′ interaction), and A=40 (wave function from Ref.,[41] AV8′ interaction). The values of the probabilities $\mathcal{P}^p_{gr(0)} = 4\pi \int k^2\, dk\, n^p_{gr}(k)$ and $\mathcal{P}^p_{ex(1)} = 4\pi \int k^2\, dk\, n^p_{ex}$, Eq.(32), are listed in Table 2 and the partial probabilities, Eq. (34), in Table 3. (Figure reprinted from.[42] Copyright (2013) by the American Physical Society)

with

$$\mathcal{P}_{gr(0)} + \mathcal{P}_{ex(1)} = 1, \tag{33}$$

yield, respectively, the probability to find a MF and a correlated nucleon in the range $0 \le k_1 \le \infty$; they can therefore be assumed as the MF and SRC total probabilities. It is clear that both low- and high-momentum components contribute to mean-field and correlated momentum distributions but, as it should be expected, $n_{gr(0)}$ ($n_{ex(1)}$) should get contribution mainly from low (high) momentum components. This is clearly illustrated in Fig. 7, where the proton momentum distributions of A=3, 4, 16, and 40 nuclei are shown with the separation into the MF and correlation contributions: it can be seen that, starting from $k \gtrsim 2\, fm^{-1}$, the momentum distributions are dominated by the correlated part. The calculated values of $\mathcal{P}_{gr(0)}$ and $\mathcal{P}_{ex(1)}$ for several nuclei are listed in Table 2. Assuming that $n_0^{N_1}$ and $n_1^{N_1}$ could be obtained from some measurable cross section, it might well be that only a

MEAN FIELD AND SRC PROBABILITIES			
Nucleus	*Potential*	$\mathcal{P}_{gr}$	$\mathcal{P}_{ex}$
^{3}He[30]	AV18[5]	0.677	0.323
^{4}He[31,32]	RSC[3] AV8′[6]	0.8	0.2
Nucleus	*Potential*	$\mathcal{P}_0$	$\mathcal{P}_1$
^{16}O[41]	V8’[6]	0.8	0.2
^{40}Ca[41]	V8’[6]	0.8	0.2

Table 2. The proton MF, $\mathcal{P}^p_{gr(0)} = \int d\,\mathbf{k}_1\, n^p_{gr(0)}(\boldsymbol{k}_1)$, and SRC, $\mathcal{P}^p_{ex(1)} = \int d\,\mathbf{k}_1\, n^p_{ex(1)}(\boldsymbol{k}_1)$, probabilities, Eq. (32), in various nuclei obtained from AV18 and AV8’ interactions. (Table reprinted from.[42] Copyright (2013) by the American Physical Society).

	^{2}H	^{3}He(p)		^{4}He		^{16}O		^{40}Ca	
k_1^-	$\mathcal{P}$	$\mathcal{P}_{gr}$	$\mathcal{P}_{ex}$	$\mathcal{P}_{gr}$	$\mathcal{P}_{ex}$	$\mathcal{P}_0$	$\mathcal{P}_1$	$\mathcal{P}_0$	$\mathcal{P}_1$
0.0	1.0	0.7	0.3	0.8	0.2	0.8	0.2	0.8	0.2
0.5	0.3	0.3	0.2	0.5	0.1	0.7	0.2	0.7	0.2
1.0	0.08	0.03	0.07	0.1	0.1	0.2	0.1	0.2	0.1
1.5	0.06	0.005	0.04	0.008	0.08	0.008	0.1	0.01	0.1
2.0	0.04	0.002	0.02	$7 \cdot 10^{-4}$	0.06	$6 \cdot 10^{-4}$	0.06	$3 \cdot 10^{-4}$	0.07

Table 3. The values of the proton partial probability, Eq. (34), for ^{3}He, ^{4}He, ^{16}O and ^{40}Ca, calculated for different values of the momentum k_1^- (in fm^{-1}) with $k_1^+ = \infty$. (Table reprinted from.[42] Copyright (2013) by the American Physical Society).

limited range of momenta is available experimentally, in which case it is useful to define the partial probabilities

$$\mathcal{P}_{0(1)}(k_1^{\pm}) = 4\,\pi \int_{k_1^-}^{k_1^+} n_{0(1)}(\boldsymbol{k}_1) k_1^2\, d\, k_1 \tag{34}$$

i.e. the probability to observe a MF or a correlated nucleon with momentum in the range $k_1^- \leq k_1 \leq k_1^+$. The calculated values of $\mathcal{P}^{N_1}_{0(1)}(k_1^{\pm})$ are given in Table 3.

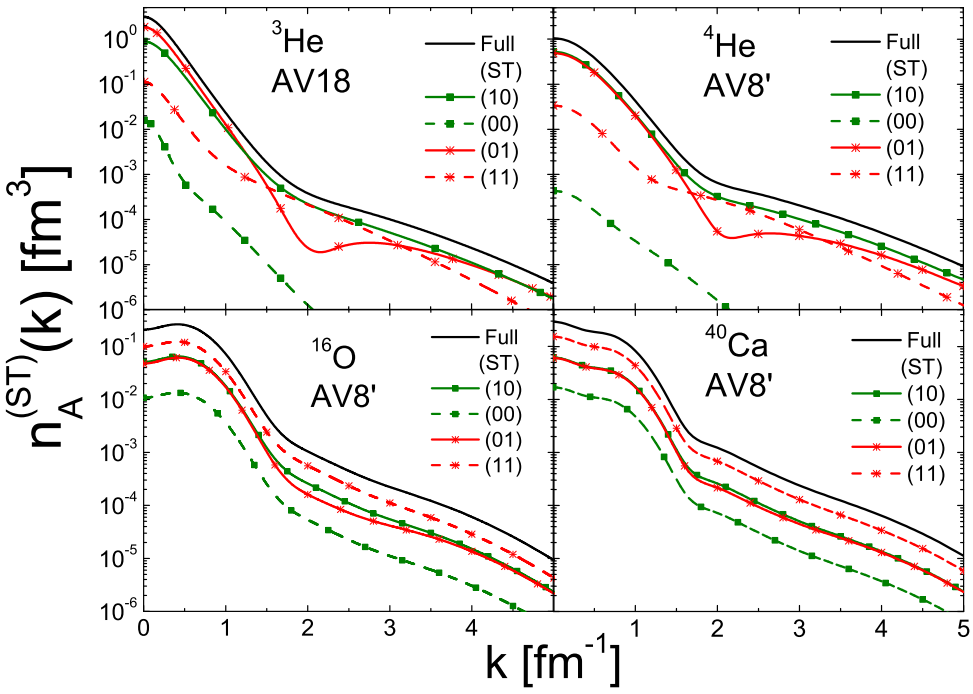

Fig. 8. The various spin-isospin contributions to the proton distributions in ^{3}He, ^{4}He, ^{16}O and ^{40}Ca (Eq. (34)). Wave functions as in Fig. 6. (Figure reprinted from.[42] Copyright (2013) by the American Physical Society)

4.4. *The spin-isospin structure of the one-body momentum distributions*

By introducing the spin-isospin dependent half-diagonal density matrix $\rho^{N_1N_2}_{(ST)}(\boldsymbol{r}_1, \boldsymbol{r}'_1; \boldsymbol{r}_2)$, the one-body momentum distribution can be expressed in terms of its various spin-isospin components as follows[42]

$$n_A(\boldsymbol{k}_1) = \sum_{(ST)} n_A^{(ST)}(\boldsymbol{k}_1) = \int d\boldsymbol{r}_1\, d\boldsymbol{r}'_1 e^{i\,\boldsymbol{k}_1\cdot(\boldsymbol{r}_1-\boldsymbol{r}'_1)} \sum_{(ST)} \int d\boldsymbol{r}_2 \rho^{N_1N_2}_{(ST)}(\boldsymbol{r}_1, \boldsymbol{r}'_1; \boldsymbol{r}_2). \quad (35)$$

In Ref.[42] the spin-isospin dependent half-diagonal two-body density has been calculated for A=3, 4, 16 and 40, and the various spin-isospin contributions to $n_A(k)$ have been obtained as shown in Fig. 8. It appears that: (i) the contribution from the (00) state is negligible, both in few-nucleon systems and complex nuclei; (ii) the contribution from the (11) state in ^{3}He and ^{4}He is small, both at low and large values of k, but it plays a relevant role in the region $1.5 \lesssim k \lesssim 2.5\, fm^{-1}$; (iii) in the proton distribution of ^{3}He the (01) contribution is important everywhere except in

the region $1.5 \lesssim k \lesssim 3\, fm^{-1}$; (iv) in complex nuclei, in agreement with the results shown in Table 1, the (11) state (odd relative orbital momenta) plays a dominant role, both in the independent particle model and in many-body approaches. These observations are useful for understanding the material presented in the next Section.

4.5. *The momentum distribution of nuclei vs the deuteron momentum distributions*

It would appear from Fig. 6(**b**), that at $k \gtrsim 1.5 - 2\, fm^{-1}$ the proton momentum distribution in $A \geq 3$ nuclei would be nothing but the rescaled deuteron momentum distribution. Such a possibility has been quantitatively investigated in Ref.[42] by plotting the ratio $R^N_{A/D}(k) = n^N_A(k)/n_D(k)$. The results are presented in Fig. 9(**a**), which shows the proton ratio for $A \geq 3$, and in Fig. 9(**b**), which shows the proton

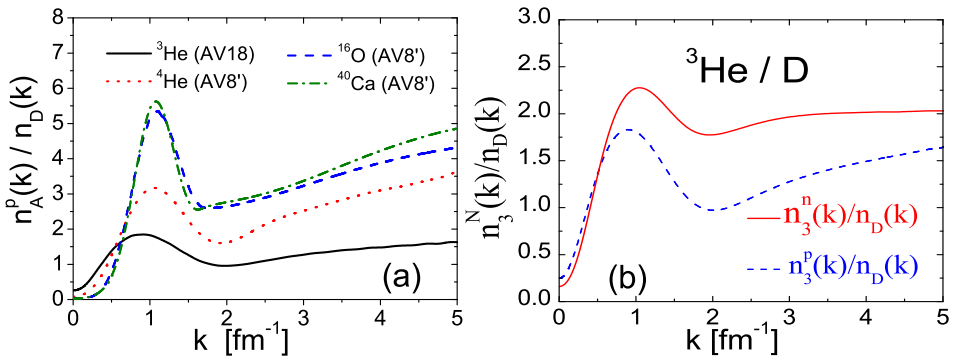

Fig. 9. (**a**): the ratio of the proton momentum distribution in nucleus A, $n^N_A(k)$, to the deuteron momentum distribution $n_D(k)$. In isoscalar nuclei $R^p_{A/D}(k) = R^n_{A/D}(k) \equiv R_{A/D}(k)$, whereas in ^{3}He $R^p_{A/D}(k) \neq n^n_A(k)/n_D(k)$. (**b**): the proton and neutron ratios in ^{3}He. Wave functions as in Fig. 6. (Figure reprinted from.[42] Copyright (2013) by the American Physical Society)

and neutron ratios in ^{3}He. The linear scale demonstrates that, starting from $k \gtrsim 2\, fm^{-1}$, the ratio $R^N_{A/D}(k)$ is not constant but appreciably increases with k. The reasons for such an increase are manyfold, namely:[42] (i) the role of the states $(ST) = (01)$ and (11), that are missing in the deuteron; (ii) the *c.m.* motion of a pair in a nucleus, that, unlike what happens in the deuteron, is not zero; (iii) the different role played by *pp* and *pn* SRCs. In order to better understand the last point, let us analyze in detail the proton and neutron momentum distributions in ^{3}He.

4.6. *The nucleon momentum distributions in ^{3}He and ^{3}H*

The different behavior of the proton and neutron momentum ratios shown in Fig. 9(**a**), can be understood in terms of SRC as follows.[42] A *pn* pair can be either in

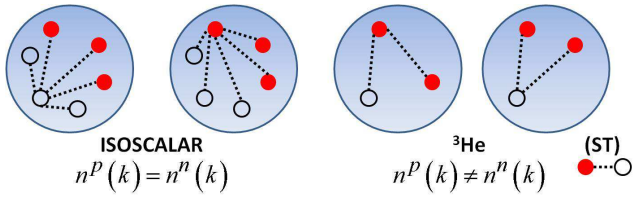

Fig. 10. The number of *pn* and *pp* pairs affecting the high-momentum components of the nucleon momentum distributions. In isoscalar nuclei $n^p(k) = n^n(k)$, whereas in non isoscalar nuclei, e.g. in ^{3}He, $n^p(k) \neq n^n(k)$ because the proton and the neutron are correlated with different nucleon pairs.(Full (open) dots denotes protons(neutrons).

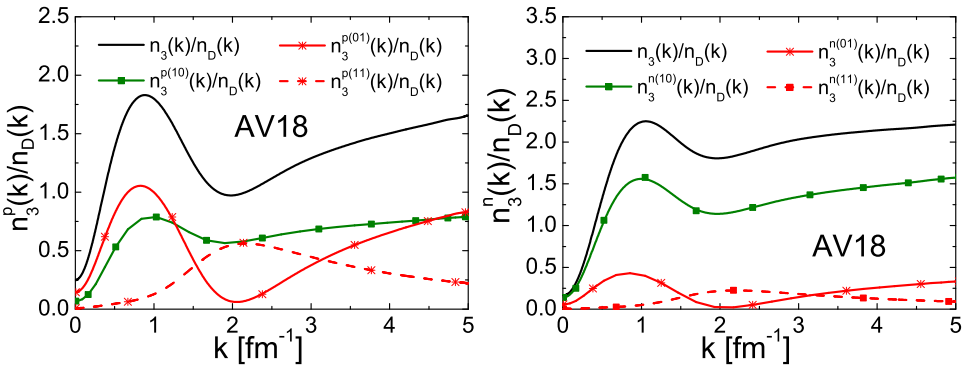

Fig. 11. The spin-isospin components of the proton (**Left**) and neutron (**Right**) ratios $n_A^N(k)/n_D(k) = \sum_{ST} n_3^{N,(ST)}(k)/n_D(k)$ in ^{3}He. Wave functions from Ref.[30] (Figure reprinted from.[42] Copyright (2013) by the American Physical Society).

deuteron-like (10) state with probability 3/4, or in (01) state, with probability 1/4; a *pp* (*nn*) pair can only be in (01) state with probability one. [a] As illustrated in the cartoon in Fig 10, in ^{3}He the proton momentum distribution is affected by SRCs acting in one *pn* and one *pp* pairs; in the former pair the deuteron-like state (10) is three times larger than the (01) state, whereas in the latter pair the deuteron-like state is totally missing; on the contrary, the neutron distribution is affected by SRCs acting in two proton-neutron pairs, with a pronounced dominance of the deuteron-like state (10); therefore, one expects that around $k \simeq 2\, fm^{-1}$, where *np* SRCs dominate over *pp* SRCs,[53–55] $n_3^n/n_D \simeq 2$ and $n_3^p/n_D \simeq 1$, which is indeed confirmed by the results presented in Fig. 11, where the various spin-isospin ratios $R_{A/D}^{N,(ST)}(k) = n_A^{N,(ST)}(k)/n_D(k)$ are presented.

[a]This is strictly true in the independent particle picture. SRCs change these probability according to the results presented in Table 1 without, however, affecting the correctness of our argument.

4.7. *Experimental evidence of high-momentum components in the one-body momentum distributions*

As already pointed out in Section 1, it is not the aim of the present review to discuss the experimental investigation and the evidence of SRCs, in particular, how the

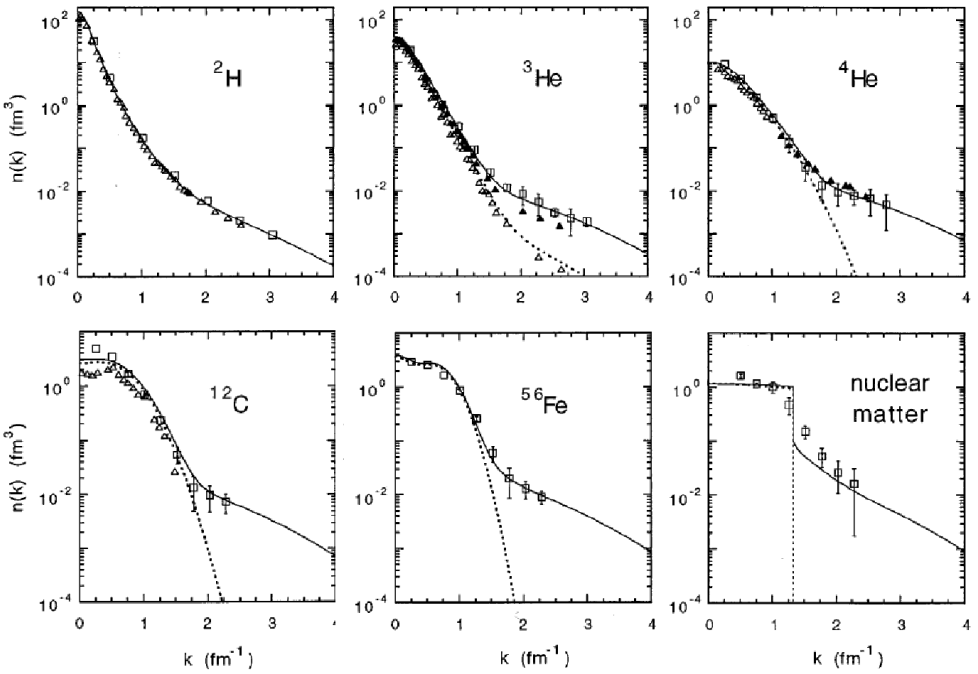

Fig. 12. The momentum distributions of several nuclei and nuclear matter extracted from the analysis of inclusive, $A(e,e')X$ (open squares), and exclusive, $A(e,e'p)X$ (full and open triangles), cross sections. The full lines represent the results of many-body calculations, as in the previous Figures, and the dashed lines are MF predictions. For references to the original experimental and theoretical papers see Ref.[56](Figure reprinted from.[56] Copyright (1991) by Elsevier)

information on momentum distributions could be extracted from different types of measured cross sections which might be strongly affected by competitive effects, like the final state interaction (FSI) and meson exchange currents (MEC). Nonetheless it is useful mentioning some established evidence of high-momentum components in $n_A(k)$. To this end, we show in Fig. 12 the one-body momentum distributions extracted from the exclusive, $A(e,e'p)X$, and inclusive, $A(e,e')X$, reactions, the latter analyzed in terms of y-scaling.[56] The y-scaling analysis produce large errors, but even in the worst case, it unambiguously demonstrates the dominant role played by SRCs in the high-momentum part of the one-body momentum distributions. Other evidence of SRCs from inclusive electron scattering is provided by the ratio of inclusive cross sections, e.g. $\sigma_A(x_{Bj},Q^2)/\sigma_D(x_{Bj},Q^2)$, plotted *vs.* the Bjorken

scaling variable x_{Bj} (see Ref.[57,58] and the review paper[2]).

5. Two-body momentum distributions

Introducing the relative and *c.m.* momenta,

$$\boldsymbol{k}_{rel} = \frac{1}{2}\,(\,\boldsymbol{k}_1 - \boldsymbol{k}_2\,) \equiv \boldsymbol{k} \qquad \boldsymbol{K}_{c.m.} = \boldsymbol{k}_1 + \boldsymbol{k}_2 \equiv \boldsymbol{K}, \tag{36}$$

the two-body momentum distribution is defined as follows

$$\begin{aligned} &n(\boldsymbol{k}_1, \boldsymbol{k}_2) = n(\boldsymbol{k}, \boldsymbol{K}) = n(k, K, \Theta) = \\ &= \frac{1}{(2\pi)^6} \int d\boldsymbol{r} d\boldsymbol{r}' d\boldsymbol{R} d\boldsymbol{R}'\, e^{-i\,\boldsymbol{K}\cdot(\boldsymbol{R}-\boldsymbol{R}')}\, e^{-i\,\boldsymbol{k}\cdot(\boldsymbol{r}-\boldsymbol{r}')} \rho(\boldsymbol{r}, \boldsymbol{r}'; \boldsymbol{R}, \boldsymbol{R}'), \end{aligned} \tag{37}$$

where $\rho(\boldsymbol{r}, \boldsymbol{r}'; \boldsymbol{R}, \boldsymbol{R}')$ is the non-diagonal two-body density (Eq. (12)), $k = |\boldsymbol{k}|$, $K = |\boldsymbol{K}|$ and Θ is the angle between $\mathbf{k}$ and $\mathbf{K}$. Three different types of two-body momentum distribution can thus be considered, namely:

(1) the relative, $n_{rel}(k)$, and *c.m.*, $n_{c.m.}(K)$, momentum distributions, i.e. Eq. (37) integrated over the *c.m.* and relative momenta, respectively:

$$n_{rel}(\boldsymbol{k}) = \frac{1}{(2\pi)^3} \int n(\boldsymbol{k}, \boldsymbol{K})\, d\boldsymbol{K} \qquad n_{c.m.}(\boldsymbol{K}) = \frac{1}{(2\pi)^3} \int n(\boldsymbol{k}, \boldsymbol{K})\, d\boldsymbol{k}; \tag{38}$$

(2) Eq. (37) in correspondence of $K_{c.m.} = 0$, describing back-to-back nucleons, as in the deuteron ($\boldsymbol{k}_2 = -\boldsymbol{k}_1$) :

$$n(\boldsymbol{k}, 0) = \frac{1}{(2\pi)^6} \int d\boldsymbol{r} d\boldsymbol{r}'\; e^{-i\,\boldsymbol{k}\cdot(\boldsymbol{r}-\boldsymbol{r}')} \int d\boldsymbol{R} d\boldsymbol{R}'\, \rho(\boldsymbol{r}, \boldsymbol{r}'; \boldsymbol{R}, \boldsymbol{R}'); \tag{39}$$

(3) the full Eq. (37) as a function of k, K and Θ, a quantity that provides a three-dimensional picture of the two-body momentum distributions.

Hereafter, the two-body momentum distributions for a pair of nucleons N_1N_2 in spin-isospin state (ST) will be denoted by $n^{N_1N_2}_{(ST)}(\boldsymbol{k}, \boldsymbol{K})$.

5.1. *The momentum distributions $n_{rel}(k)$ and $n_{c.m.}(K)$*

Fig. 13(**Left**) shows the relative and *c.m.* momentum distributions in ^{4}He obtained in Ref.[54] whereas Fig. 13(**Right**) shows the the relative momentum distributions for *pn* pairs in state $(ST) = (10)$ in ^{2}H, ^{3}He, ^{3}H, ^{4}He and^{4}He* from Ref.[44] Both calculation are *ab initio* within the VMC method with the AV18 interaction (Ref.[54]) and the correlated basis approach with the AV8$'$ interaction (Ref.[44]). The inset in Fig. 13 illustrates the dominance of the tensor force acting in *pn* pairs: at low momenta, the ratio $n_{np}(k)/n_{pp}(k)$ is mostly governed by the ratio of the *pn* to *pp* pairs, $ZN/[Z(Z-1)/2] = 2$ but starting from $k \geq 1.5\, fm^{-1}$, the ratio sharply increases because of the action of the tensor force in the (10) channel of the *np* pair. The results exhibited in Fig. 13 demonstrate the universality of SRCs in few-nucleon system: at high values of k, the relative momentum distributions are very similar,

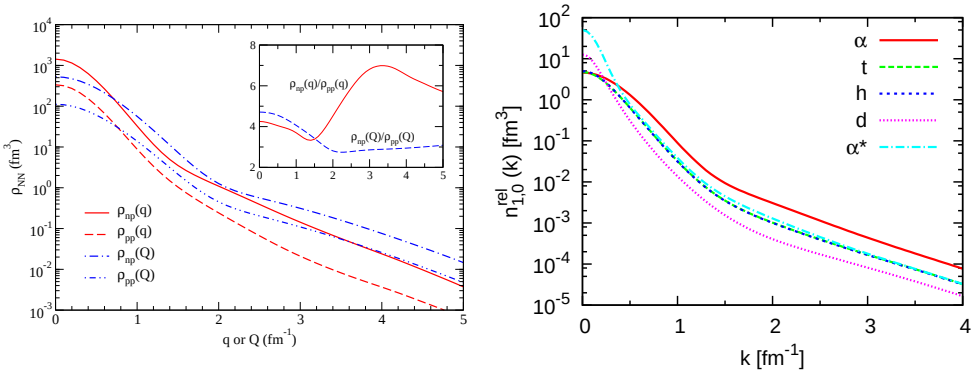

Fig. 13. (Color online) (**Left**): the two-body momentum distribution of np and pp pairs in ^{4}He, integrated over the the *c.m.* (relative) momentum $K \equiv Q$ ($k \equiv q$) *vs.* the relative (c.m.) momentum (Eq. (38)), with $n_{rel}(k) \equiv \rho_{NN}(q)$ and $n_{c.m.}(K) \equiv \rho_{NN}(Q)$. The inset shows the ratios $\rho_{np}(q)/\rho_{pp}(q)$ and $\rho_{np}(Q)/\rho_{pp}(Q)$. (Figure reprinted from.[54] Copyright (2007) by the American Physical Society). (**Right**): the same as in Fig. 13(**Left**) for a pair in $S = 1, T = 0$ channel in ^{2}H $\equiv$ d, ^{3}He $\equiv$ h, ^{3}H $\equiv$ t, ^{4}He $\equiv \alpha$ and ^{4}He$^* \equiv \alpha^*$. (Figure reprinted from.[44] Copyright (2011) by the American Physical Society).

thanks to the universality of the correlation hole previously discussed in Section 2.3. The universality of the integrated momentum distributions is confirmed by the results for A=12, 16 and 40, obtained in Ref.[45] within the number-conserving linked-cluster expansion and the AV8′ NN interaction.

5.2. *The momentum distributions* $n(k_{rel}, K_{c.m.} = 0)$

The momentum distribution $n(k_{rel}, K_{c.m.} = 0)$ is a very important quantity because, when compared with the deuteron momentum distribution, it can provide information on the short-range dynamics of a pair of nucleons in the medium and possible evidence of medium induced multi-nucleon correlations.

The results for A=3, 4, 6 and 8 nuclei, obtained in Ref.[54] within the VMC method using different NN interactions plus 3N forces, are shown in Fig. 14, whereas the results for A=12, 16 and 40, obtained in Ref.[55] within the number-conserving linked-cluster expansion and the AV8′ NN interaction, are shown in Fig. 15. The results for both few-nucleon systems and complex nuclei clearly show that: (i) the 3NF, which is essential to produce the correct binding energy of few-nucleon systems, appears to have tiny effects on the high-momentum components (Fig. 14(**Left**)), which is not surprising, in view of its long-range character; (ii) the universality of the relative momentum distributions, resulting from the universality of SRCs, is evident from Fig. 14(**Right**) and Fig. 15(**a**): in the range $3 \leq A \leq 40$ and $k \geq 2\, fm^{-1}$ a clear A-independence of the high relative-momentum behavior is exhibited; (iii) the results presented in Figs. 13(**a**) and 15(**b**) demonstrate the tensor dominance both in few-nucleon systems and complex nuclei; (iv) Fig. 14(**Left**) and 15(**b**) shows that at high values of k_{rel} the momentum distributions of deuteron

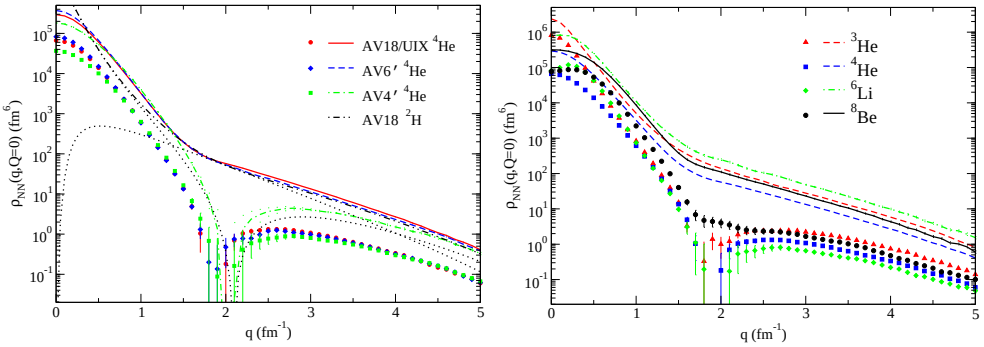

Fig. 14. (Color online) (**Left**): the two-body momentum distributions of back-to-back nucleons (Eq. (39) with $K_{c.m.} \equiv Q = 0$ and $n(k,0) \equiv \rho(q, Q = 0)$) for np pairs (lines) and pp pairs (symbols) in ^{4}He, calculated with VMC wave functions and different NN interactions: AV18 plus UIX three nucleon interaction,[28] AV6′[7] and AV4′[7] interactions. The dotted lines denote the S and D waves of the deuteron corresponding to the AV18 interaction. (**Right**): the same as in (**Left**) but for ^{3}He, ^{4}He, ^{6}Li, and ^{8}Be. AV18 interaction.(Figure reprinted from.[54] Copyright (2007) by the American Physical Society)

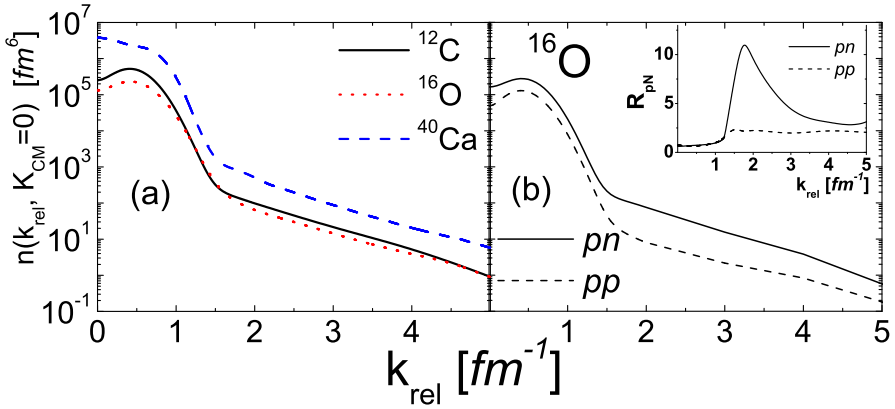

Fig. 15. (Color online) (**a**): the two-nucleon momentum distribution in ^{12}C, ^{16}O and ^{40}Ca for back-to-back nucleons (Eq. (39)) calculated within the number-conserving linked-cluster expansion of Ref.[41] with AV8' interaction. (**b**): the back-to-back pn and pp momentum distributions in ^{16}O. The inset shows the ratio of the total momentum distributions to the distributions obtained by disregarding the tensor force, i.e. $R_{pN} = n_{pN}(k_{rel}, K_{c.m.} = 0)/n_{pN}^{central}(k_{rel}, K_{c.m.} = 0)$. All curves are normalization to the number of NN pair. (Figure reprinted from.[55] Copyright (2008) by the American Physical Society)

and complex nucleus are very similar. This similarity is better illustrated in the next Section where the ratio $R_{A/D}(k, K_{c.m.} = 0) = n_A^{pn}(k_{rel}, K_{c.m.} = 0)/n_D(k)$ is presented for few-nucleon systems and complex nuclei.

5.3. *The momentum distributions* $n(k_{rel}, K_{c.m.}, \Theta)$

The knowledge of $n(k_{rel}, K_{c.m.}, \Theta)$ provides information on the three-dimensional picture of the two-nucleon momentum distribution. In this connection, it has to be stressed that the independence of $n(k_{rel}, K_{c.m.}, \Theta)$ upon the angle Θ is evidence of the factorization of the distributions in variables $k_{\rm rel}$ and $K_{\rm c.m.}$,[59,60] i.e. $n^{NN}(k_{\rm rel}, K_{\rm c.m.}, \Theta) \Rightarrow \phi(k_{\rm rel})\chi(K_{\rm c.m.})$ where, for the time being, $\phi(k_{\rm rel})$ and $\chi(K_{\rm c.m.})$ denote two generic functions of k_{rel} and $K_{c.m.}$. The pn and pp two-body momentum distributions $n(k_{rel}, K_{c.m.}, \Theta)$ in few-nucleon systems[59] and complex nuclei[45] have been calculated with realistic wave functions. The results for ^{3}He and ^{4}He obtained with *ab initio* wave functions[30,31] corresponding to the $AV18$[5] and $AV8'$[6] interactions are shown in Fig. 16 *vs.* $k_{\rm rel}$, in correspondence of several values of $K_{\rm c.m.}$ and two values of Θ. The results for ^{16}O are shown in Fig. 17.

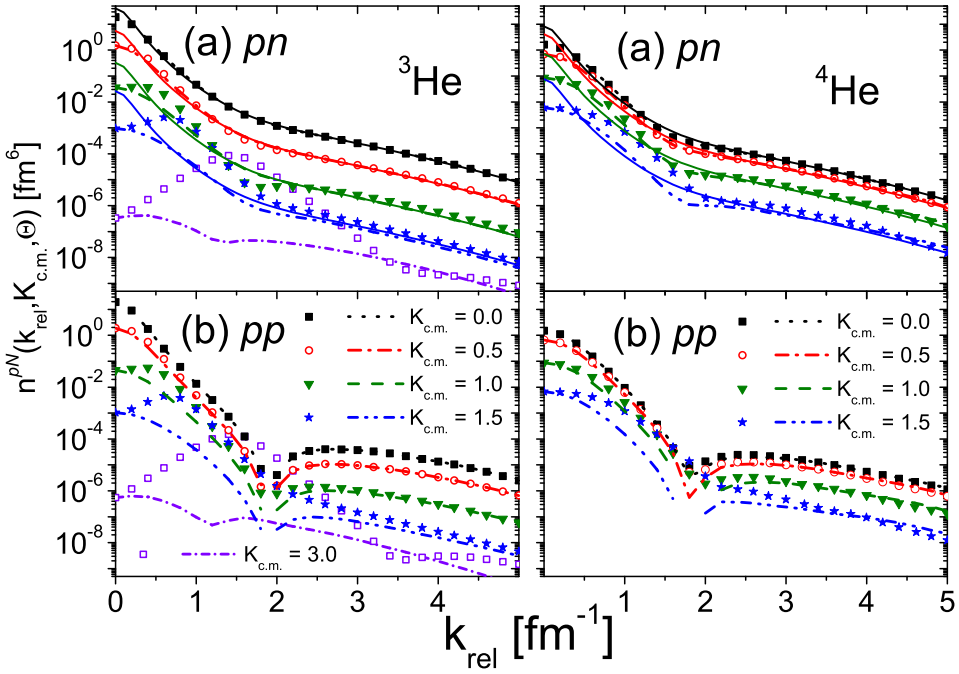

Fig. 16. (Color online) (**Left**): the two-body momentum distributions of pn (**a**) and pp (**b**) pairs in ^{3}He normalized to unity, *vs.* the relative momentum k_{rel}, for fixed values of the c.m. momentum $K_{c.m.}$ and two orientations of the momenta, namely $\mathbf{k}_{rel}||\mathbf{K}_{c.m.}$ (*broken curves*) and $\mathbf{k}_{rel} \perp \mathbf{K}_{c.m.}$ (*symbols*). The continuous curves for the pn pair represents the deuteron momentum distribution rescaled by the c.m. momentum distribution $n^{pn}_{c.m.}(K_{c.m.}) = \int n^{pn}(\boldsymbol{k}_{rel}, \boldsymbol{K}_{c.m.})\, d\boldsymbol{k}_{rel}$ (see Eq. (37)). ^{3}He wave function from Ref.[30] and $AV18$ interaction.[5] (**Right**): the same as in (**Left**) but for ^4He. Correlated variational wave function from[31] and $AV8'$ interaction.[6](Figure reprinted from.[59] Copyright (2012) by the American Physical Society)

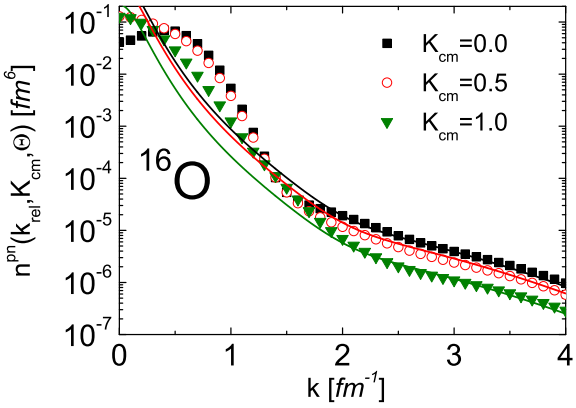

Fig. 17. The two-body proton-neutron momentum distributions (Eq. (37)) in ^{16}O for three values of $K_{c.m.}$ and $\Theta = 0$ (symbols). The continuous lines represent the deuteron momentum distributions rescaled by the c.m. momentum distribution of the pair calculated at the proper value of K_{cm} (see Fig. 18(**b**)). Wave function from the number-conserved linked-cluster expansion of Ref.[41] AV8′ NN interaction. (Figure adapted from.[55] Copyright (2008) by the American Physical Society)

Apart from a different overall normalization, the results for few-nucleon systems at

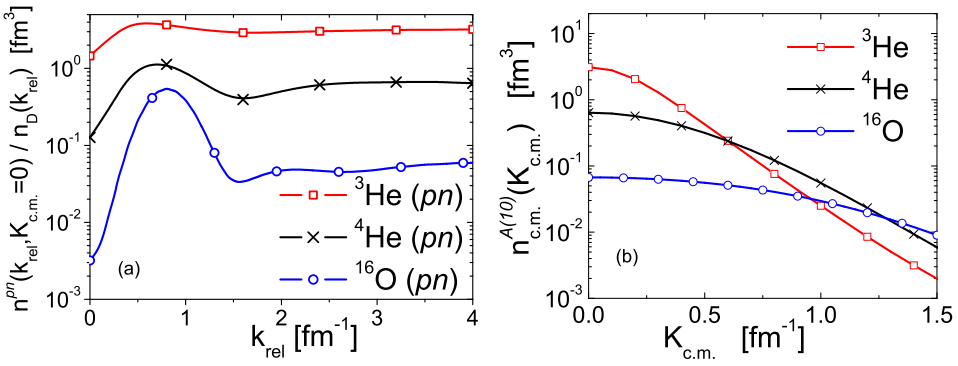

Fig. 18. (**a**): the ratio of the *pn* momentum distributions for back-to-back nucleons $n^{pn}(k_{\rm rel}, K_{\rm c.m.} = 0)$ in ^{3}He,^{4}He, and ^{16}O shown in Figs. 16 and 17, to the deuteron momentum distribution $n_D(k_{\rm rel})$ (full lines). The different magnitudes of the ratio for the three nuclei is due to the different values of the c.m. momentum distribution at $K_{\rm c.m.} = 0$ shown in Fig.18(**b**). (**b**): the *c.m.* momentum distribution in ^{3}He, ^4He, and ^{16}O. (Figure reprinted from.[42,59] Copyright (2012,2013) by the American Physical Society)

$K_{\rm c.m.} = 0$ fully agree with the ones of Ref.[54] The peculiar and systematic results of

these calculations can be summarized as follows: (i) with increasing values of the c.m. momentum, the high relative momentum part of the distributions strongly decreases; (ii) starting from a given value of $k_{\rm rel}$, being $k_{\rm rel} \simeq 1.5$ fm^{-1} when $K_{\rm c.m.} = 0$ and assuming increasing values with increasing values of $K_{\rm c.m.}$, the *pn* distribution changes its slope and becomes close to the deuteron distribution. In particular, in the region ($k_{\rm rel} \gtrsim 2\,$fm^{-1}, $K_{\rm c.m.} \lesssim 1$ fm^{-1}), n^{pn} becomes Θ-independent[b], assuming the form $n^{pn}(k_{\rm rel}, K_{\rm c.m.}, \Theta) \simeq n_D(k_{\rm rel}) n^{pn}_{\rm c.m.}(K_{\rm c.m.})$, where $n_D(k_{\rm rel})$ is the deuteron momentum distribution, and $n^{pn}_{\rm c.m.}(K_{\rm c.m.})$ describes the c.m. motion of the pair and provides the A-dependence of $n^{pn}(k_{\rm rel}, K_{\rm c.m.})$. The factorized property, that charaterizes also complex nuclei, as shown in the case of ^{16}O in Fig. 17, represents a rigorous many-body demonstration that when the relative momentum of the *pn* pair is high, and, at the same time, the c.m. momentum is low, the two-body momentum distribution factorizes; (iii) when the *c.m.* momentum is of the same order of the (high) relative momentum, more than two particles can be locally correlated, with a resulting strong dependence upon the angle and the breaking down of factorization, as clearly appears in Fig. 16 for $K_{\rm c.m.} = 3$ fm^{-1}. These feature are common to both few-nucleon systems and complex nuclei. A better evidence on the factorized behavior of the two-body momentum distributions for *pn* pairs can be obtained by considering the ratio $R^{pn}(k) = n^{pn}(k_{\rm rel}, 0)/n_D(k_{\rm rel})$, which is presented in Fig. 18(**a**). The constant value exhibited by the ratio at $k_{\rm rel} \gtrsim 1.5$ fm^{-1} is unquestionable evidence that in this region the dependence upon $k_{\rm rel}$ of the two-body momentum distribution $n^{pn}(k_{\rm rel}, 0)$ is the same as in the deuteron. As for the different magnitudes of the ratio for different nuclei, this is governed by the c.m. motion distribution of the pair, which is illustrated in Fig. 18(**b**). It can be seen that the difference in magnitude of the ratios in the region $k_{\rm rel} \gtrsim 1.5$ fm^{-1} is governed by exactly the difference between the values of the *c.m.* momentum distributions at $K_{\rm c.m.} = 0$. The more rapid fall off of the *c.m.* momentum distributions of ^{3}He, is due to the weak binding of this nucleus, leading, with respect to the ^{4}He and ^{16}O, to the wider separation of the curves corresponding to various values of $K_{\rm c.m.}$ presented in Figs. 16 and 18(**a**). For nuclei with $A \geq 4$ and $K_{\rm c.m.} \lesssim 1.0 - 1.5$ fm^{-1}, the *c.m.* distribution can be associated to the average kinetic energy $< T >_{SM}$ of a pair moving in the mean field with a Gaussian distribution , $n_{c.m.}(K) \propto \exp\{-\alpha K^2_{c.m.}\}$ with $\alpha = 3/[2 < K^2_{c.m.} >] = [3(A-1)]/[4(A-2) m_N < T_{SM} >]$ as suggested in Ref.[49] and in agreement with the experimental finding[61] for ^{12}C.

6. Nucleon momentum distributions, spectral functions and SRCs

Although the momentum distribution is not an observable, it is undisputable that it can play a role in particular scattering processes, that, at the same time, can also be influenced by other phenomena which could mask the effects generated by the momentum distributions. To clarify this point, let us consider the process

[b]Such an independence has been checked in a wide range of angles

$A(e,e'N)X$ in the Plane Wave Impulse Approximation (PWIA), i.e. when, in the initial state, an electron is impinging on nucleus A and, in the final state, the scattered electron and a nucleon N are detected in coincidence and the nucleus $X = (A-1)$ is left in the energy state E^f_{A-1}; in the simplified assumption that the detected nucleon was knocked out by a direct interaction $\gamma^* N$ and left the nucleus with momentum $\mathbf{p}_N$ without interacting with the medium, the measurable missing momentum $\mathbf{p}_m = \mathbf{q} - \mathbf{p}_N$ and energy $E_m = \nu - T_N - T_{A-1}$ represent, respectively, the momentum of the nucleon before interaction $\mathbf{k}_1 = -\mathbf{p_m}$ and the intrinsic excitation energy of E^*_{A-1} of $(A-1)$. As is well known, even within such a severe approximation the cross section of the process is not proportional to the momentum distribution but to another quantity, the Spectral Function $S_A(\mathbf{k}_1, E)$ representing the joint probability that when a nucleon with momentum $\mathbf{k}_1 = -\mathbf{p}_m$ is removed instantaneously from the ground state of the nucleus A, the nucleus $(A-1)$ is left in the excited state $E^*_{A-1} = E - E_{min}$, where E is the removal energy and $E_{min} = M_{A-1} + m_N - M_A$. The spectral function has the following form (from now-on spin indexes will be omitted for ease of presentation)

$$
\begin{aligned}
S_A(\boldsymbol{k}_1, E) &= < \Psi^A_0 | a^\dagger_{\mathbf{k}_1} \delta(E - \hat{H} + E_A) a_{\mathbf{k}_1} | \Psi^A_0 > = \\
&= \sum_f \Big| \int e^{i\boldsymbol{k}_1 \cdot \boldsymbol{r}_1} d\,\boldsymbol{r}_1 \int \Psi^{(A-1)\,*}_f(\{\boldsymbol{r}\}_{A-1}) \Psi^A_0(\boldsymbol{r}_1, \{\boldsymbol{r}\}_{A-1}) \prod_{i=2}^{A} d\,\boldsymbol{r}_i \Big|^2 \delta(E - E^f_{A-1} + E_A) \\
&= S_{gr(0)}(\boldsymbol{k}_1, E_{gr(0)}) + S_{ex(1)}(\boldsymbol{k}_1, E_{ex(1)})
\end{aligned}
\tag{40}
$$

where $E^f_{A-1} = E_{A-1} + E^*_{A-1}$, E_A and E_{A-1} denote the ground-state energies of initial and final nuclei, and $a^\dagger_{\boldsymbol{k}_1}(a_{\boldsymbol{k}_1})$ is a creation (annihilation) operator. The two contributions, as in the case of the momentum distributions (cf. Eqs. (25) and (28)), arise from different final states of the system $(A-1)$, with $S_{ex(1)}(\boldsymbol{k}_1, E)$ governed by SRCs. Summing over the complete set of final states in Eq. (40) it is easy to obtain the *momentum sum rule*

$$
n_A(\boldsymbol{k}_1) = \int_0^\infty S_A(\boldsymbol{k}_1, E)\, d\,E. \tag{41}
$$

Eq. (41) clearly shows that the extraction of the momentum distribution from the experimental data implies a difficult integration over the full range of discrete and continuum excitation spectra of the residual nucleus $(A-1)$, up to very high values of E^*_{A-1}, particularly in the interesting region of high values of k (see Ref.[50–52]). Moreover, exact many-body spectral functions exist only for the three-nucleon system,[62–64] (the complete set of final state is known), and for nuclear matter,[65,66] whereas for complex nuclei only model spectral functions have been developed, either within the local density approximation,[67] or within the convolution model of Ref.[49] The latter, which is aimed at describing the spectral function in the region of 2N SRCs, naturally arises from the behavior of the high-momentum part of the two-body momentum distributions described in the previous Sections. As a matter of fact, we have seen that at large values of k_{rel} and small values of $K_{c.m.}$ the

following relation holds

$$n^{pn}(\mathbf{k}_{rel},\mathbf{K}_{c.m.}) \simeq n^{pn}(k_{rel},K_{c.m.}) \simeq n_D(k_{rel}) n_{c.m.}(K_{c.m.}). \quad (42)$$

From momentum conservation, $\mathbf{k}_1 + \mathbf{k}_2 - \mathbf{K}_{c.m.} = 0$, $\mathbf{k}_{rel} = \mathbf{k}_1 - \mathbf{K}_{c.m.}/2$, one has

$$n_A(k_1) \simeq \int n_D(|\boldsymbol{k}_1 - \frac{\boldsymbol{K}_{c.m.}}{2}|) n_{c.m.}(K_{c.m.})\, d\,\boldsymbol{K}_{c.m.} = \int S_A(k_1,E)\, d\,E, \quad (43)$$

and assuming that the high values of the excitation energy E^*_{A-1} are essentially given by the relative motion of nucleon "2" and nucleus $(A-2)$, one obtains

$$S_A(k_1,E) \simeq \int n_D(|\boldsymbol{k}_1 - \frac{\boldsymbol{K}^N_{c.m.}}{2}|) n^N_{c.m.}(K_{c.m.}) d\,\boldsymbol{K}_{c.m.} \times \\ \times\, \delta\left(E - E^{(2)}_{th} - \frac{A-2}{2m_N(A-1)}\left[\boldsymbol{k}_1 - \frac{A-1}{A-2}\boldsymbol{K}_{c.m.}\right]^2\right), \quad (44)$$

where $E^{(2)}_{th}$ is the two-body threshold. Eq. (44) has been first obtained in Ref.,[49] within several phenomenological assumptions, whose physical correctness are now justified by the many-body calculation of the momentum distributions. A convolution formula for the correlated part of the spectral function has also been shown to result from Brueckner-Bethe-Goldstone theory of nuclear matter, where the spectral function corresponding to the nucleon self-energy $M(k,E) = V(k,S) + iW(k,E)$ is obtained from the single particle Green function $\mathcal{G}$ in the following form[68]

$$S_A(k,E) = -\frac{1}{\pi} Im\mathcal{G}(k,E) = \frac{1}{\pi}\frac{W(k,E)}{\left(-E - k^2/2m_N - V(k,E)\right)^2 + W(k,E)^2} \quad (45)$$

which, at $E + \frac{k^2}{2m_N} >> |V(k,E)|; |W(k,E)|$, can be approximated by the following convolution integral[69]

$$S_A(k_1,E) = \frac{\pi^2\,\rho}{16}\int \frac{d^3\,\mathbf{K}_{c.m.}}{(2\pi)^3} n_{rel}(|\mathbf{k}_1 - \frac{1}{2}\mathbf{K}_{c.m.}|) n^{FG}_{c.m.}(K_{c.m.}) \times \\ \times\, \delta\left(E - E^{(2)}_{thr} - \frac{1}{2\,m_N}(\mathbf{K}_{c.m.} - \mathbf{k}_1)^2\right). \quad (46)$$

Here ρ is the density of nuclear matter, $n^{FG}_{c.m.}$ the Fermi gas distribution and n_{rel} the spin-isospin averaged two-body relative momentum distribution in nuclear matter. Eq. (46) in the region $E \simeq E^{(2)}_{thr} + k^2/(2m_N)$ agrees very well with the exact BBG spectral function, as shown in Fig. 19(**a**). Further confirmation of the convolution model, resulting from the factorization property of $n(\boldsymbol{k}_{rel},\boldsymbol{K}_{c.m.})$, has been recently provided[60] by the analysis of the behavior of *ab initio* three-nucleon ground-state wave functions Ψ_0 in momentum space, by considering the following ratio

$$R = \frac{|\Psi_0(\mathbf{K}_{cm},\mathbf{k}_{rel})|^2}{|\Psi_0(\mathbf{K}_{cm}=0,\mathbf{k}_{rel})|^2}, \quad (47)$$

vs. $|\boldsymbol{k_{rel}}|$ at constant values of $|\boldsymbol{K_{c.m.}}|$. If factorization of Ψ_0 holds, i.e. $|\Psi_0(\mathbf{K}_{cm}, \mathbf{k}_{rel})|^2 \simeq n_{c.m.}(K_{c.m.}) n_{rel}(k_{rel})$ the ratio becomes

$$R \simeq \frac{n_{c.m.}(K_{c.m.})}{n_{c.m.}(K_{c.m.}=0)} = constant. \tag{48}$$

It can be seen from Fig. 19(**b**) that factorization indeed occurs starting, as expected,

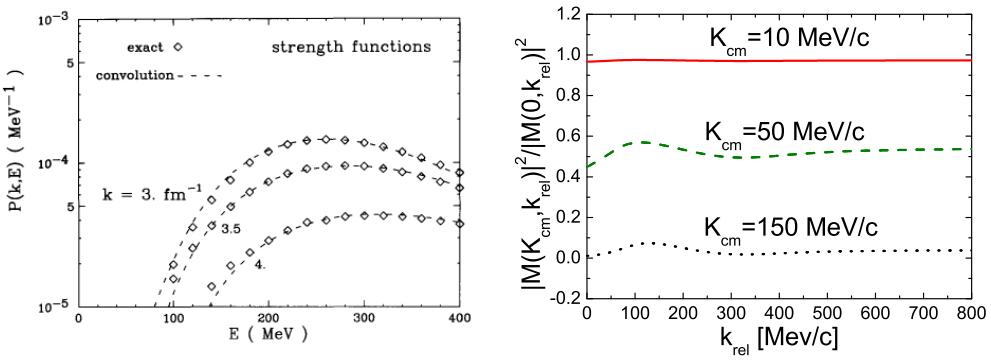

Fig. 19. (**Left**): the exact BBG nuclear matter spectral function (*exact*) *vs* E in correspondence of three values of k compared with the BBG convolution model Eq.(46)(*convolution*). (Figure reprinted from.[69] Copyright (1996) by Elsevier). (**Right**): the ratio R (Eq. (47)) in ^{3}He. Three-nucleon wave functions from Ref.[30] AV18 interaction.[5](Figure reprinted from.[60] Copyright (2011) by Springer & Verlag).

at a value of k_{rel} which increases with increasing values of $K_{c.m.}$, in agreement with the results presented in Fig. 16. The magnitudes of the curves in Fig. 19(**b**) agree with the behavior of $n_{c.m.}(K_{c.m.})$ presented in Fig. 18.

The most interesting quantity, as far as SRCs are concerned, is the two-nucleon momentum distributions, that in PWIA might in principle be extracted from the $A(e,e'2N)X$ process, when two nucleons are knocked out from the nucleus A and are detected with momenta $\mathbf{p}_1$ and $\mathbf{p}_2$ in coincidence with the scattered electron, with the nucleus $(A-2)$ left in the energy state E^f_{A-2}. The measurable missing momentum and energy are in this case the $\mathbf{p}_m = \mathbf{q} - \mathbf{p}_1 - \mathbf{p}_2$ and $E_m = \nu - T_{p_1} - T_{p_2} - T_{A-2} = E^*_{A-2}$. Assuming that the virtual photon has interacted with one nucleon (the fast one) of a correlated pair, with the second nucleon (the recoiling one) being emitted because of momentum conservation, the cross section will depend upon the two-nucleon spectral function

$$S_A^{N_1 N_2}(\boldsymbol{k}_1, \boldsymbol{k}_2, E) = < \Psi_0 | a^\dagger_{\mathbf{k}_1} a^\dagger_{\mathbf{k}_2} \delta(E - \hat{H} + E_A) a_{\mathbf{k}_2} a_{\mathbf{k}_1} | \Psi_0 > =$$
$$\sum_f \Big| \int e^{-i\boldsymbol{k}_1 \cdot \boldsymbol{r}_1 - i\boldsymbol{k}_2 \cdot \boldsymbol{r}_2} d\,\boldsymbol{r}_1 d\,\boldsymbol{r}_2 \langle \Psi_f^{(A-2)*}(\{\mathbf{r}\}_{A-2}) | \Psi_0(\mathbf{r}_1, \mathbf{r}_2 \{\mathbf{r}\}_{A-2}) \rangle \times$$
$$\times \delta(E - E^f_{A-2} + E_A). \tag{49}$$

Summing over the final states of $(A-2)$ the *two-nucleon momentum sum rule*

$$n_A^{N_1N_2}(\boldsymbol{k}_1,\boldsymbol{k}_2) = \int d\,E\, S_A^{N_1N_2}(\boldsymbol{k}_1,\boldsymbol{k}_2,E) = n(k_{rel},K_{c.m.},\Theta) \tag{50}$$

is obtained. The two-nucleon Spectral Functions has been obtained within many body theories in Refs.[70] for finite nuclei, in Ref.[71] for nuclear matter, and in Ref.[72] for ^{3}He [c]. In the past, the process $A(e,e'N_1N_2)X$ has been intensively investigated theoretically (see e.g.,[73,74] and references therein quoted) and experimentally (see e.g.[75] and references therein quoted) but the experimental data were plagued by MEC and FSI and other competing effects and no conclusive quantitative information on SRCs could be obtained (for a critical discussion of this topic see[2]). Recently, however, high moment transfer experiments have been performed on ^{12}C and ^{4}He[61,76–78] that allowed one to detect a "fast" proton with momentum $\mathbf{p}_1$, identified as the member of a correlated pair kicked out by the high energy projectile, and a "slow" (or "recoil") nucleon (a proton or a neutron) with momentum $\mathbf{p}_2$, assumed to be the one emitted by momentum conservation in the correlated pair. By assuming the validity of the PWIA, which implies that $\mathbf{p}_1 = \mathbf{k}_1 + \mathbf{q}$, $\mathbf{p}_2 = \mathbf{k}_2$ and $\mathbf{P}_{mis} = -(\mathbf{k}_1+\mathbf{k}_2) = \mathbf{K}_{c.m.}$, it is possible to reconstruct the momentum $\mathbf{k}_1$ that the struck nucleon had before interaction; by plotting the correlation between the value of $|\mathbf{p}_2|$ and the angle between $\mathbf{k}_1$ and $\mathbf{p}_2$, it was found that whereas recoiling nucleons with momentum of the order or less than the Fermi momentum were emitted isotropically, nucleons with momentum $p_2 \simeq 2-2.5\,fm^{-1}$ were emitted in a backward cone with respect to the direction of $\mathbf{k}_1$, in agreement with the picture of the absorption of the virtual photon by a nucleon with a *c.m.* distribution in ^{12}C of the type $n_{c.m.}(K) \propto \exp[-K^2_{c.m.}/2\sigma^2]$ with $\sigma = 7.26 \pm 0.086\,fm^{-1}$ in agreement with the prediction of Ref.,[49] namely $\sigma = 1/\sqrt{2\alpha} = 7.1\,fm^{-1}$ (see Section 5.3). Furthermore by comparing with the same apparatus and kinematics the yield of $^{12}C(e,e'p)X$ with the yield of $^{12}C(e,e'pn)X$ it has been possible to obtain information about the ratio of *pn* to *pp* correlated pairs. A detailed discussion of these experiments and their interpretation is given in Ref.[2]

7. Conclusions

Ab initio many-body calculations performed in terms of realistic bare two-nucleon interactions show that two-nucleon short-range correlations (2N SRCs), characterized by the presence of a correlation hole in the two-nucleon density in nuclei, exhibit a universal character, manifesting itself in several A-independent features of nucleon momentum distributions. As a matter of fact, the calculated two-nucleon relative density displays a correlation hole which is essentially independent of the mass of the nucleus, a feature that demonstrates that two-nucleon motion at short relative distances is practically unaffected by the motion of nearby nucleons. This

[c] Eq. (49) has been called *vector spectral function* in Ref.[72] whereas a similar quantity has been called *decay function* in Ref.[2]

universal behavior in coordinate space reflects itself in peculiar universal features of one-nucleon, $n_A(|\mathbf{k}|)$, and two-nucleon, $n^{N_1N_2}(|\mathbf{k}_{rel}|, |\mathbf{K}_{c.m.}|, \Theta)$, momentum distributions. Concerning $n_A(|\mathbf{k}|)$, 2N SRCs increase the high-momentum part by orders of magnitude with respect to MF predictions; as for $n^{N_1N_2}(|\mathbf{k}_{rel}|, |\mathbf{K}_{c.m.}|, \Theta)$, particularly worth being stressed again is the following main feature characterizing the motion of a *pn* pair in medium: in the SRCs region, where $2 \lesssim k_{\rm rel} \lesssim 5$ fm^{-1} and, at the same time, $K_{\rm c.m.} \lesssim 1$ fm^{-1}, the relative and *c.m.* motions of the pair are decoupled, with the former described by a deuteron-like momentum distribution, and the latter, governing the A dependence of the motion, described by a momentum distribution linked to the average value of the MF kinetic energy. Such a decoupling of the relative and *c.m.* momenta have been theoretically justified by many-body calculations which predict factorization of the nuclear wave function at short internucleon distances or, equivalently, at high values of k_{rel} and low values of $K_{c.m.}$. Some aspects of this picture have already been partially confirmed by experiments providing evidence on the high-momentum content of the one-nucleon momentum distribution, by the experimental behavior of the inclusive electron-nucleus cross section ratios and, eventually, by the measurement of the percentage ratio of *pn* to *pp* correlated pairs in ^{4}He and ^{12}C. Much work however remains to be done in order to investigate the three-dimensional structure of the two-nucleon momentum distributions $n^{N_1N_2}(|\mathbf{k}_{rel}|, |\mathbf{K}_{c.m.}|, \Theta)$, with particular attention to its *c.m.* dependence in the SRCs region, as well as to its structure in the region where both k_{rel} and $K_{c.m.}$ are large, characterized by the breaking down of c.m and relative momenta factorization due to the expected dominant role of many-nucleon SRCs.

Unveiling the correlation structure of nuclei is a fundamental task of nuclear physics, for by this way information on the basic in-medium NN interaction can be obtained. Moreover, it should also be stressed that, recently, a non trivial impact of 2N SRCs on different fields, such as high-energy hadron-nucleus[79–81] and nucleus-nucleus scattering,[82] deep inelastic scattering[83] and the equation of state of unconventional nuclear matter,[84,85] has been demonstrated.

References

1. A. Bohr, B. N. Mottelson, *Nuclear Structure*, World Scientific (1969).
2. J. Arrington, D. W. Higinbotham, G. Rosner, and M. Sargsian, *Prog. in Part. and Nucl. Phys.* **67** (2012) 898.
3. R.V. Reid, *Ann. Phys. N.Y.* **50** (1968) 411.
4. M. Lacombe *et al.*, *Phys. Rev.* **C 21** (1980), 861.
5. R. B. Wiringa, V. G. J. Stoks and R. Schiavilla, *Phys. Rev.* **C51** (1995) 38.
6. B. S. Pudliner *et al*, *Phys. Rev.* **C56** (1997) 1720.
7. R. B. Wiringa and S. C. Pieper, *Phys. Rev. Lett.* **8**9 (2002) 182501.
8. R. Machleidt, and D. R. Entem, *Phys. Rep* **503**(2011)1.
9. E. Epelbaum, H.-W. Hammer and U.-G Meissner, *Rev. Mod. Phys.* **81** (2009) 1773.
10. W. N. Polizou and W. Glöckle, *Few-Body Systems* **9** (1990) 97.
11. J. P. Vary, *Phys. Rev.* C**7**, (1973) 521.
12. R. Roth, T. Neff and H. Feldmeier, *Prog. Part. Nucl. Phys.* **65** (2010) 50.

13. B. R. Barrett, P. Navrtil and J. P. Vary, *Progr. in Part. and Nucl. Phys.* **69** (2013) 131.
14. K. Suzuki and S. Y. Lee, *Progr. Theor. Phys.* **64** (1980) 2091.
15. S. K. Bogner, R. J. Furnstahl and A. Schwenk, *Prog. Part. Nucl. Phys.* **65** (2010) 94.
16. S. K. Bogner, T. T. S. Kuo and A. Schwenk, *Phys. Rep.* **386** (2003) 1.
17. E. R. Anderson, S. K. Bogner, R. J. Furnstahl and R. J. Perry, *Phys. Rev.* **C82** (2010) 054001.
18. S. K. Bogner and D. Roscher, *Phys. Rev.* **C86** (2012) 064304.
19. R. J. Furnstahal and K. Hebeler, arXiv:1305.3800v1 [nucl-th] (2013).
20. J. W. Holt, N. Kaiser and W. Weise, arXiv:1304.6350v1 [nucl-th] (2013).
21. R. Jastrow, *Phys. Rev.* **98** (1955) 1479.
22. K. Gottfried, *Annals of Physics* **21** (1963) 29.
23. H. Primakoff, T. Holstein, *Phys. Rev.* **55** (1939) 1218.
24. A. Nogga, H. Kamada, W. Gloeckle, *Phys. Rev. Lett.* **785** (2000) 944.
25. A. Kievsky, M. Viviani, L. Girlanda and L.E. Marcucci, *Phys. Rev.* **C81** (2010) 044003.
26. S. C. Pieper, and R. B. Wiringa, *Annu. Rev. Nucl. Part. Sci.* **51** (2011) 53.
27. H.-W. Hammer, A. Nogga, and A. Schwenk, *Rev. Mod. Phys.* **85** (2013) 197.
28. B. S. Pudliner *et al*, *Phys. Rev. Lett.* **7**3 (1995) 4396.
29. W. Gloeckle, H. Witala, D. Huber, H. Kamada and J. Golak, *Phys. Rept.* **274** (1996) 107.
30. A. Kievsky, S. Rosati, M. Viviani, *Nucl. Phys.* **A551** (1993) 241.
L.E. Marcucci, L. Girlanda, A. Kievsky, S. Rosati and M. Viviani, *Few-Body Syst.* **44** (2008) 227.
31. H. Morita, Y. Akaishi, H. Tanaka, *Prog. Theor. Phys.* **79** (1988) 863.
H. Morita *et al*, to be published
32. R. Schiavilla, V. R. Pandharipande, R. B. Wiringa, *Nucl. Phys.* **A449** (1986) 219.
33. K. Varga and Y Suzuki, *Stochastic Variational Approach to Quantum-Mechanical Few-Body Problems*, Lecture Notes in Physics **54** (Springer, 1998)
34. K. Varga and Y. Suzuki, *Phys. Rev.* **C52** (1995) 2885.
35. Y.Suzuki and H. Horiuchi, *Nucl. Phys.* **A81** (2009) 188.
36. V. Efros, W. Leidemann and G. Orlandini, *Few-Body. Syst.* **14** (1993) 151.
37. W. Leidemann and G. Orlandini, *Prog. in Part. and Nucl. Phys.* **68** (2013) 158.
38. S. C. Pieper, *Rivista Nuovo Cimento* 31 (2008) 709.
39. S. C. Pieper, R. B. Wiringa and V. R. Pandharipande, *Phys. Rev.* **C46** (1992) 1741.
40. F. Arias de Saavedra, C. Bisconti, G. Co' and A. Fabrocini, *Phys. Rep.* **450** (2007) 1.
41. M. Alvioli, C. Ciofi degli Atti and H. Morita, *Phys. Rev.* **C72** (2005) 054310.
42. M. Alvioli, C. Ciofi degli Atti, L. P. Kaptari, C. B. Mezzetti and H. Morita, *Phys. Rev.* **C87** (2013) 034603.
43. H. Kamada, A. Nogga, W. Gloeckle *et al*, *Phys. Rev.* **C64** (2001) 044001.
44. H. Feldmeier, W. Horiuchi, T. Neff and Y. Suzuki, *Phys. Rev.* **C84** (2011) 054003 .
45. M. Alvioli, C. Ciofi degli Atti and H.Morita, ArXiv: 0709:3989 (2007).
46. J. L. Forest, V. R. Pandharipande, S. C. Pieper, R. B. Wiringa, R. Schiavilla and A. Arriaga, *Phys. Rev.* **C54** (1996) 646.
47. L. L. Frankfurt, M. I. Strikman, *Phys. Rept.* **160** (1988) 235.
48. J. G. Zabolitzki and W. Ey, *Phys. Lett.* **B76** (1978) 527.
49. C. Ciofi degli Atti, S. Simula, *Phys. Rev.* **C53** (1996) 1689.
50. C. Ciofi degli Atti, E. Pace and G. Salmè, *Phys. Lett.* **B141** (1984) 14.

51. C. Ciofi degli Atti and S. Liuti, *Phys. Lett.* **B225** (1989) 215.
52. C. Ciofi degli Atti, S. Liuti and S. Simula, *Phys. Rev.* **C41** (1990) R2474.
53. M. M. Sargsian, T. V. Abrahamyan, M. I. Strikman and L. L. Frankfurt, *Pys. Rev.* **C71** (2005) 044615.
54. R. Schiavilla, R. B. Wiringa, S. C. Pieper and J. Carlson, *Phys. Rev. Lett.* **98** (2007) 132501.
55. M. Alvioli, C. Ciofi degli Atti and H. Morita, *Phys. Rev. Lett.* **100**(2008) 162503.
56. C. Ciofi degli Atti, E. Pace and G. Salme, *Phys. Rev.* **C43** (1991) 1155.
57. N. Fomin *et al.*, *Phys. Rev. Lett.* **108** (2012) 092502.
58. C. Ciofi degli Atti and C. B. Mezzetti, *Phys. Rev.* **C79** (2009) R051302.
59. M. Alvioli, C. Ciofi degli Atti, L. P. Kaptari, C. B. Mezzetti, H. Morita and S. Scopetta, *Phys. Rev.* **C85** (2012) 021001.
60. C. Ciofi degli Atti, L. P Kaptari, H. Morita and S. Scopetta, *Few-Body Systems* **50**(2011) 243.
61. A. Tang, J. W. Watson, J. L. S. Aclander, J. Alster, G. Asryan, *et al.*, *Phys. Rev. Lett.* **90** (2003) 042301.
62. A. Dieperink, T. de Forest, I. Sick, and R. Brandenburg, *Phys. Lett.* **B63** (1976) 261.
63. C. Ciofi degli Atti, E. Pace, and G. Salmè, *Phys. Rev.* **C21** (1980) 805.
64. H. Meier-Hajduk, C. Hajduk, P. Sauer and W. Theis, *Nucl. Phys.* **A395**, (1983) 332.
65. O. Benhar, A. Fabrocini and S. Fantoni, *Nucl. Phys.* **A505**, (1989) 267.
66. A. Ramos , A. Polls and W. Dickhoff, *Nucl. Phys.* **A503** (1989) 1.
67. O. Benhar, A. Fabrocini, S. Fantoni, and I. Sick, *Nucl. Phys.* **A579** (1994) 493.
68. W. H. Dickhoff and D. Van Neck, *Many-Body Theory Exposed!*, World Scientific, 2007.
69. M. Baldo, M. Borromeo and C. Ciofi degli Atti, *Nucl. Phys.* **A604** (1996) 429.
70. W. J. W. Geurts, K. Allart, W. H. Dickhoff and H. Müther, *Phys. Rev.* **C54** (1996) 1144.
71. O. Benhar and A. Fabrocini, *Phys. Rev.* **C62** (2000) 034304.
72. C. Ciofi degli Atti, L. P. Kaptari, *Phys. Rev.* **C66** (2002) 044004.
73. J. Ryckebusch, M. Vanderhaegen, K. Heyde and M. Varoquier, *Phys. Lett.* **B350** (1995) 1.
74. C. Giusti, F. D. Pacati, M. Schwamb and S. Boffi, *Eur. Phys. J.* **A33** (2007) 29.
75. D. L. Groep *et al.*, *Phys. Rev.* **C63** (2001) 014005.
76. E. Piasetzky *et al*, *Phys. Rev. Lett.* **97** (2006) 162504.
77. R. Shneor, *et al.*, *Phys. Rev. Lett.* **99** (2007) 072501.
78. R. Subedi *et al.*, *Science* **320** (2008) 1476.
79. M. Alvioli, C. Ciofi degli Atti, H. Morita, I. Marchino and V. Palli, *Phys. Rev.* **C78** (2008) 031601(R).
80. M. Alvioli, C. Ciofi degli Atti, B. Z. Kopeliovich, I. K. Potashnikova and I. Schmidt, *Phys. Rev.* **C81** (2010) 025204.
81. C. Ciofi degli Atti, B. Z. Kopeliovich, C. B. Mezzetti, I. K. Potashnikova and I. Schmidt, *Phys. Rev.* **C84** (2011) 025205.
82. M. Alvioli, M. Strikman, *Phys. Rev.* **C83** (2011) 044905.
83. O. Hen, D. W. Higinbotham, G. A. Miller, E. Piasetzky and L. B. Weinstein, to appear in *Int. J. Mod. Phys.E*, ArXiv:1304:2813v1 [nucl-th] (2013).
84. T. Frick, H. Muther, A. Rios, A. Polls and A. Ramos, *Phys. Rev.* **C71**(2005) 014313.
85. L. Frankfurt, M. Sargsian and M. Strikman, *Int. J. Mod. Phys.* **A23** (2008) 2991.